J Cancer Res Clin Oncol (2010) 136:717–736
DOI 10.1007/s00432-009-0711-4

ORIGINAL PAPER

Features of senescence and cell death induced by doxorubicin in A549 cells: organization and level of selected cytoskeletal proteins

Anna Litwiniec · Alina Grzanka · Anna Helmin-Basa · Lidia Gackowska · Dariusz Grzanka

Received: 26 March 2009 / Accepted: 19 October 2009 / Published online: 7 November 2009

Abstract
Purpose Senescence and cell death are fail-safe mechanisms protecting against tumorigenesis. Both these forms of cellular response could be induced in cancer cells, thus suppressing tumor progression. Therefore, to fully understand chemotherapeutic effects, not only symptoms of cell death, but also of senescence should be evaluated. Since the involvement of cytoskeleton components in these processes has been reported, changes in the organization and level of some cytoskeletal proteins may be indicative of cell fate.
Methods We analyzed selected markers of senescence and cell death, including possible alterations in vimentin and G-actin cytoskeleton in A549 cells after treatment with doxorubicin. Light (SA-β-galactosidase), fluorescent (vimentin and G-actin labeling) and electron microscopic examinations along with flow cytometry methods (TUNEL, Annexin V/PI staining, cell cycle analysis, intracellular level of vimentin) were employed to determine the outcome of the treatment.
Results Uncoupling between senescent cell morphology and stable cell cycle arrest occurred. Some differences in the organization and level of cytoskeletal proteins, especially of vimentin, like fluctuations in its level, were observed. On the other hand, G-actin seemed to be more stable than vimentin.
Conclusions G-actin stability may imply its potential usefulness for permanent senescence detection. Along with slight to moderate cytoskeletal alterations, the obtained results suggest transient senescence-like state induction, followed by morphology typical of mitotic catastrophe in part of the A549 cells.

Keywords Senescence · Cell death · Doxorubicin · Vimentin · G-actin

A. Litwiniec (✉) · A. Grzanka
Department of Histology and Embryology, Ludwik Rydygier Collegium Medicum in Bydgoszcz, Nicolaus Copernicus University in Toruń, Karłowicza 24, 85-092 Bydgoszcz, Poland
e-mail: annalitwiniec@wp.pl

A. Helmin-Basa · L. Gackowska
Department of Immunology, Collegium Medicum, Nicolaus Copernicus University in Toruń, Skłodowskiej-Curie 9, 85-094 Bydgoszcz, Poland

D. Grzanka
Department of Clinical Pathomorphology, Collegium Medicum, Nicolaus Copernicus University in Toruń, Skłodowskiej-Curie 9, 85-094 Bydgoszcz, Poland

Introduction

During the last decades it has become apparent that not only apoptosis, but also other modes of cell death, as well as senescence determine the outcome of cancer therapy (Schmitt et al. 2002; Amaravadi and Thompson 2007). In cell lines and mouse models with artificially induced apoptotic defects, neither clonogenic survival of cancer cells after treatment with chemotherapeutic drugs nor tumor formation was significantly enhanced, probably due to the combined effects of senescence and other non-apoptotic modes of cell death, including mitotic catastrophe (Lock and Stribinskiene 1996; Crescenzi et al. 2003; Rebbaa et al. 2003; Douarre et al. 2005; Feldser and Greider 2007). Moreover, there have been some suggestions that the senescence program on the cellular level has been established during evolution to act as a natural barrier against tumorigenesis, thus excluding cells harboring

cancer-promoting mutations from a proliferating population in benign lesions (Braig et al. 2005; Chen et al. 2005; Michaloglou et al. 2005). Analogically, there has been a growing body of evidence from in vitro and in vivo experiments that stress-induced premature senescence is a program executed by cells in response to chemotherapy (Wang et al. 1998; Chang et al. 2002; Schmitt et al. 2002; te Poele et al. 2002; Crescenzi et al. 2005). As a consequence, some suggestions regarding prognostic implications appear (te Poele et al. 2002). However, the question, if prematurely induced senescence in advanced stages of cancer could be as safe and effective approach as protective mechanisms acting at early stages of carcinogenesis, remains controversial. Therefore, before clinical applications, potential beneficial effects such as lower than pro-apoptotic and less toxic doses of cytostatics required for senescence induction, the effectiveness even in apoptotic-resistant cell clones, as well as positive in vivo results, should be weighed against possible adverse effects related to this complex phenomenon. For example, it is believed that senescence may be triggered by low sublethal doses of some drugs, but, on the other hand, a risk exists that extensive repair of damages would prevail over a stable cell cycle arrest in such case (Wang et al. 1998; Rebbaa 2005). Thus, senescence-escaped cells could be able to divide further in certain conditions (Beauséjour et al. 2003; Roberson et al. 2005).

In the present work, we analyzed not only selected symptoms of cell death, but also of senescence in non-small cell lung carcinoma A549 cells exposed to doxorubicin at a range of nanomolar concentrations. The human lung adenocarcinoma cell line A549 originates from alveolar epithelial type II cells (Giard et al. 1973). This cell line has retained many properties of type II cells of the pulmonary epithelium, including metabolic and transport features, the presence of surfactant-containing lamellar bodies, etc. (Lieber et al. 1976; Foster et al. 1998; Hukkanen et al. 2000). Concurrently, some cell subpopulations with distinct features have been identified in the original heterogeneous cell population (Hatcher et al. 1997; Croce et al. 1999). What is more, this cell line displays characteristic mutations in tumor-suppressor genes, i.e., $p16^{INK4a}$, $p14^{ARF}$ and $p15^{INK4b}$ homozygous deletions, which are common in many cancers (Okamoto et al. 1995; Iavarone and Massagué 1997; Edelman et al. 2001; Xie et al. 2005). Therefore, apart from being a valuable model for studies on human pulmonary metabolism, this cell line is also broadly used for in vitro evaluation of chemotherapeutic effectiveness and antineoplastic activities of different agents in non-small cell lung cancer (Edelman et al. 2001; Riou et al. 2002; Haynes et al. 2003; Mortenson et al. 2004; Filyak et al. 2008). In fact, this type of lung cancer is the leading cause of death from cancer worldwide (Hoffman et al. 2000; Parkin 2001, Spira and Ettinger 2004). Since in a majority of patients an unresectable advanced or metastatic disease is diagnosed at presentation, treatment regimens often comprise chemotherapy and radiotherapy (Hoffman et al. 2000). Doxorubicin is a component of some historical, but also present chemotherapeutic regimens for the treatment of NSCLC, with the reported response rate ranging from 20 to 50% (Pronzato et al. 2001; Patlakas et al. 2005; Otterson et al. 2007; Mi et al. 2008). Doxorubicin belongs to anthracyclines. This antineoplastic antibiotic acts mainly by intercalation into the DNA molecule and disruption of DNA and RNA synthesis, as well as by inhibiting of the DNA topoizomerase II and producing DNA single- and double-strand breaks (Meriwether and Bachur 1972; Binaschi et al. 1997). Some features of senescence and cell death were described in human lung adenocarcinoma A549 cells after treatment with doxorubicin (Crescenzi et al. 2005; Klein et al. 2005; Filyak et al. 2007). Here, we describe organization and level of vimentin and nuclear G-actin in A549 cell line after treatment with doxorubicin (Adriblastin), on the background of selected markers of senescence and cell death.

Senescence on the cellular level is a state of restricted proliferative capacity, even after mitogenic stimulation. At the same time, senescent cells remain metabolically active and display many characteristic features, such as enlarged and flattened morphology, enhanced activity of senescence-associated β-galactosidase, disturbances in cell cycle progression, formation of senescence-associated heterochromatin foci, alterations in the expression of tumor-suppressor genes, e.g., *p53*, $p21^{Cip1/Waf1/Sdi1}$, $p14^{Arf}$, $p16^{Ink4a}$, *pRb*, lipofuscin accumulation, increased cytoplasmic granularity and nuclear volume (Dimri et al. 1995; Fang et al. 1999; Dimri et al. 2000; Narita et al. 2003; Węsierska-Gądek et al. 2005; Zhang et al. 2007). Apart from that, polyploidy and size heterogeneity appear on the cell population level (Walen 2007).

There have also been some reports suggesting a possible involvement of cytoskeletal proteins in this phenomenon. An intermediate filament protein, vimentin was proved to be highly expressed in senescent fibroblasts (Di Felice et al. 2005; Nishio and Inoue 2005). The gene encoding this protein was also up-regulated during senescence of prostate epithelial cells (Untergasser et al. 2002). Analogically, nuclear G-actin accumulation was shown to be an early and universal marker of cellular senescence, comparably efficient to senescence-associated β-galactosidase (Kwak et al. 2004). Additionally, it was observed that interference with nuclear export of G-actin leads to a restriction of proliferative capacity, which is one of the most prominent symptoms of senescence (Wada et al. 1998; Bird et al. 2003). Alterations in

organization and level of cytoskeleton components including intermediate filaments and actin also reflect some subtle changes related to different kinds of programmed cell death (Bursch et al. 2000). Therefore, it seems that cellular levels of vimentin and G-actin might be modulated to some extent during senescence and cell death, especially if these programs are induced by DNA-damaging and oxidative stress-generating agents such as doxorubicin.

The aim of this study was to investigate possible changes in the levels, as well as the organization of vimentin and nuclear G-actin in a population of A549 cells induced to enter a senescence and/or cell death program. Moreover, we sought to determine if this cell line shows features of stable senescence after treatment with sublethal doses of the drug.

Materials and methods

Cell culture and treatment conditions

The human lung adenocarcinoma cell line A549 was kindly provided by Ph.D. P. Kopiński (Department of Gene Therapy, Ludwik Rydygier Collegium Medicum in Bydgoszcz, Nicolaus Copernicus University, Poland). Cells were routinely propagated in monolayer culture in Dulbecco's modified Eagle's medium with Glutamax (DMEM; Gibco) supplemented with 10% fetal bovine serum (FBS; Gibco) and 50 μg/ml of gentamycine (Sigma-Aldrich) at 37°C in a humidified CO_2 incubator.

Doxorubicin (Adriblastin PFS) was from Pharmacia Italia S.p.A., Pfizer Group, Milan, Italy. A stock solution of doxorubicin (2 mg/ml) was kept at 4°C. Working dilutions were performed in sterile water and were added to the cell culture at appropriate doses. Twenty-four hours after seeding, cells in the exponential phase of growth were treated with increasing concentrations of doxorubicin (50, 100, 200 nM) for 72 h. After that, the cells grew in fresh drug-free medium for further 24 h, before harvesting for the following experimental procedures.

Senescence-associated β-galactosidase assay

Senescence-associated β-galactosidase activity was detected using the Senescent Cells Staining Kit (Sigma-Aldrich), according to the manufacturer's protocols. Briefly, the cells grown on coverslips were washed with Dulbecco's PBS and fixed in a buffer including 2% formaldehyde/0.2% glutaraldehyde at room temperature for 6 min. The cells were then washed again with DPBS and incubated with a freshly prepared staining solution (pH 6) containing X-gal (5-bromo-4-chloro-3-indolyl-β-galactopyranoside) in the dark at 37°C for 20 h. After rinsing with DPBS, coverslips were mounted with Aqua Poly/Mount (Polysciences).

The percentage of blue-stained cells in the total number of cells was determined by light microscopy (Eclipse E800, Nikon). Results were presented as the mean number of cells displaying an enhanced staining with the indigogenic substrate from at least five fields for each experimental condition.

Cell cycle analysis

Cells grown on 6-well plates were trypsinized and washed with PBS. The cell suspensions in PBS ($1–2 \times 10^6$ cells/ml) were centrifuged for 5 min at $300\times g$, and the supernatant was removed. To quantify DNA content, the cell pellet was first resuspended in 1 ml of NSS solution containing 50 μg/ml PI, 0.0112% (w/v) sodium citrate (Sigma-Aldrich) and 0.03% (v/v) nonylphenylpolyethylene glycol (Nonidet P40 Substitute; Fluka). After centrifugation (5 min at $300\times g$) and supernatant removal, the cells were subsequently resuspended in 250 μl of NSS and incubated in the dark at room temperature for 15 min. Finally, 250 μl of RNase A solution (10 μg/ml RNase A in PBS) (Sigma-Aldrich) was added to each sample for a 15-min incubation in the dark at room temperature. Following addition of 0.5 ml PBS, the cells were analyzed by flow cytometry (FACScan; Becton–Dickinson). Cell cycle distribution was estimated using CellQuest software (Becton–Dickinson). For each sample, 20,000 events were acquired and the non-clumped cells were gated for further measurements. According to the DNA content, fractions of cells in G_0/G_1, S, G_2/M phases, as well as in subG_1 ($<G_1$), and cells with more than 4*n* DNA (>G2) content were determined in the whole cell population.

TUNEL assay

DNA fragmentation was measured by the terminal deoxynucleotidyl transferase-mediated dUTP nick-end labeling (TUNEL) method using a commercially available kit (APO-DIRECT, BD Biosciences Pharmingen), according to the manufacturer's instructions. In this assay, enzymatic labeling of the free 3′OH ends of the DNA with fluorescent dUTP enables double- and single-strand breaks detection. Briefly, after trypsinization, cells were fixed on ice with 1% (w/v) formaldehyde (Polysciences) in PBS for 15 min and were washed with PBS. The cells were then resuspended in 70% (v/v) ice-cold ethanol (POCh) and kept at −20°C for at least 18 h before the staining procedure. Fixed and permeabilized cells were incubated at 37°C with staining solution containing TdT enzyme and substrate (dUTP-FITC). After washing, the cells were counterstained with PI/RNase solution. Flow cytometric analysis was

performed on FACScan, using CellQuest software (Becton–Dickinson). For each sample, 20,000 events were acquired and the non-clumped cells were gated for further measurements. Cell cycle distribution was also examined in order to evaluate DNA fragmentation in each phase of the cell cycle.

Annexin V assay

To determine the extent of apoptotic and necrotic cell death, cells were stained with annexin V conjugated with FITC and PI using the Annexin V-FITC Apoptosis Detection Kit (BD Biosciences Pharmingen), according to the manufacturer's protocols. Annexin V has a high affinity for phosphatidylserine exposed on the outer membrane of apoptotic cells, while PI is transported to late-stage apoptotic/necrotic cells with disrupted cell membranes. The cells were trypsinized, washed with PBS, and resuspended in 195 µl of annexin V binding buffer with addition of 5 µl annexin V-FITC. Following incubation (for 15 min in the dark at room temperature) and centrifugation (5 min, 300 × *g*), 190 µl of annexin V binding buffer and 10 µl of PI were added to the cell pellet and incubated for further 5 min in the same conditions. Then, viable (annexin V-, PI-negative), early apoptotic (annexin V-positive, PI-negative), late apoptotic (annexin V-, PI-positive) and necrotic (annexin V-negative, PI-positive) cells were detected by flow cytometry (FACScan; Becton–Dickinson) and quantified by CellQuest software (Becton–Dickinson).

Immunofluorescence

Vimentin labeling

For labeling of vimentin, cells grown on coverslips in 12-well plates were subjected to immunofluorescence, according to previously described procedure (Safiejko-Mroczka and Bell 1998). The cells prefixed (10 min, 37°C) with 0.4 mg/ml bifunctional protein crosslinking reagent DTSP in HBSS [DTSP, 3,3′-dithio-bis(propionic acid *N*-hydroxysuccinimide ester); Hank's balanced salt solution, both from Sigma-Aldrich] were preextracted in Tsb [0.5% (w/v) Triton X-100 (Serva) in MTSB] containing 0.4 mg/ml DTSP for 10 min at 37°C and extracted in Tsb for 5 min at 37°C. After fixation with 4% (w/v) paraformaldehyde (Serva) in MTSB for 15 min at 37°C, the cells were blocked with 0.1 M glycine and incubated with 1% (w/v) bovine serum albumin (both from Sigma-Aldrich) in Tris-buffered saline, pH 7.6 (BSA-TBS), 2 × 5 min. Incubation with mouse monoclonal anti-vimentin antibody (clone V9; Sigma-Aldrich) in BSA-TBS (1:200) was performed for 45 min at 37°C in a moist chamber. After rinsing with BSA-TBS, 3 × 5 min, the cells were incubated with TRITC-conjugated goat anti-mouse IgG (Sigma-Aldrich) in BSA-TBS (1:85) in the same conditions as before. Finally, the coverslips were washed twice with BSA-TBS, washed with PBS, counterstained with diaminophenyl indole (DAPI; Sigma-Aldrich), washed again, 3 × 5 min, and mounted with Aqua Poly/Mount (Polysciences).

G-actin labeling

Two methods were employed for G-actin fluorescent staining, i.e., with DNaseI and with vitamin D-binding protein. In the first mentioned method, cells grown on coverslips were permeabilized and fixed identically like that in the procedure of vimentin staining. After fixation step, the cells were incubated with 0.1 M glycine in DPBS for 5 min at room temperature and washed twice for 5 min with DPBS. Then, the cells were blocked with 2 µM phalloidin (Sigma-Aldrich) in DPBS and incubated with DNase I-Alexa Fluor 488 conjugate (Molecular Probes) in DPBS (1:50) for 20 min in the dark. Following washing with PBS and staining with DAPI, the coverslips were washed again, 3 × 5 min, and mounted on glass slides with Aqua Poly/Mount (Polysciences).

The second, indirect procedure for staining of non-filamentous actin was performed as previously described (Cao et al. 1993; Meijerman et al. 1997; Akisaka et al. 2001). Cells grown on coverslips were washed with PBS and fixed with 3.7% (w/v) paraformaldehyde (Serva) in PBS for 20 min at room temperature. Fixed cells were washed with PBS, 3 × 5 min, and incubated with the addition of 1 mg/ml $NaBH_4$ (Sigma-Aldrich) in PBS for 10 min at room temperature in order to reduce free aldehyde groups. Then, the cells were washed with PBS, 3 × 5 min, extracted in 0.1% (w/v) Triton X-100 in PBS and incubated for 10 min with 0.1% (w/v) Triton X-100 and 0.2% (w/v) BSA in PBS (PBS-TB). For visualization of G-actin, the coverslips were subjected to subsequent incubation steps: with 10 µg/ml vitamin D-binding protein (DBP; Calbiochem) in PBS-TB for 60 min at room temperature, with goat polyclonal anti-DBP IgG (Santa Cruz Biotechnology) in PBS-TB (1:50) for 60 min at room temperature, and with Alexa Fluor 488-conjugated donkey anti-goat IgG (Molecular Probes) in PBS-TB (1:100) for 60 min at 37°C in a moist chamber. These steps were split and followed by washing with PBS-TB, 3 × 5 min. Afterward, the coverslips were washed twice with PBS, counterstained with DAPI, washed again with PBS, 3 × 5 min, and mounted with Aqua Poly/Mount (Polysciences).

All fluorescent images were obtained and analyzed using an Eclipse E800 microscope (Nikon) and NIS Elements AR imaging software (Nikon).

Flow cytometric analysis of vimentin expression

Cells grown on 6-well plates were trypsinized, washed with PBS, centrifuged (5 min, 300×*g*) and resuspended at a final concentration of 1–2 × 10^6cells/ml in 1 ml PBS with addition of 100 µl of formaldehyde (Polysciences). After incubation on ice for 15 min in the dark and subsequent centrifugation (5 min, 300×*g*), the cell pellet was permeabilized by the addition of 2 ml of ice-cold 50% (v/v) methanol (JT Baker). The cells were incubated for 15 min on ice, washed twice with cold PBS and resuspended in 100 µl of PBS. For intracellular staining, the cell suspensions were transferred into flow cytometric tubes containing 20 µl of PE-conjugated mouse monoclonal anti-vimentin IgG_1 (clone V9) or normal mouse IgG_1-PE as an isotype control (both from Santa Cruz Biotechnology). Following a 30-min incubation on ice and washing with PBS, the cells were centrifuged for 5 min at 500×*g* to wash off excess antibody, and were resuspended in 200 µl of PBS for flow cytometric analysis on FACScan (Becton–Dickinson). CellQuest software (Becton–Dickinson) was used to calculate the percentage of vimentin-positive cells and the mean fluorescence intensity of these cells for each experimental case.

Quantitative immunofluorescence assay: nuclear level of G-actin

For analysis of nuclear G-actin content, isolation of nuclei was performed in order to avoid contamination by cytoplasmic actin. After trypsinization, washing with PBS and centrifugation (5 min, 300×*g*), 2 ml of homogenizing buffer [50 mM Tris–HCl, pH 7.5; 0.3 M sucrose; 15 mM $CaCl_2$; 25 mM $MgCl_2$; 10.01 mM 2-metcaptoethanol (all from Sigma-Aldrich); 0.5% (v/v) Nonidet P40 Substitute] were added to each sample. The suspensions homogenized on ice were then centrifuged (10 min, 1,000×*g*) and the supernatant was decanted. The pellet resuspended in 1 ml of homogenizing buffer was gently stratified on top of the buffer for purification of nuclei [10 mM Tris–HCl; 0.3 M sucrose; 25 mM $MgCl_2$; 25 mM KCl; 10.01 mM 2-mercaptoethanol (all from Sigma-Aldrich); 41% (v/v) glycerol (Roth)] in fresh tubes (8 ml). Following centrifugation (10 min, 1,000×*g*), the nuclei were washed with PBS, fixed in 3.7% (w/v) paraformaldehyde (Serva), cytocentrifuged on glass slides and processed for fluorescent staining, according to the method with the use of vitamin D-binding protein as described above.

Finally, digital images obtained by fluorescence microscopy (Eclipse E800; Nikon) were imported to ImageJ software (National Institutes of Health) and converted to grayscale (8-bit). Thereafter G-actin fluorescence was colocalized with DAPI and subtracted by the nucleus area. Mean fluorescence intensity was measured and expressed as the mean grey value, that is defined as the average grey value for all pixels within the indicated area.

Transmission electron microscopy (TEM)

For observation of cell morphology and ultrastructure, cells seeded on 6-well plates were harvested by trypsinization and fixed with 2.5% (v/v) glutaraldehyde (Merck) in 0.1 M sodium cacodylate (Fluka), pH 7.4, for 30 min at room temperature. After washing in cacodylate buffer, a fibrin clot with cells entrapped was formed from bovine thrombin (Biomed) and fibrinogen (Fluka), postfixed with 2% (w/v) OsO_4 (Serva) in 0.1 M cacodylate buffer for 1 h at room temperature, passed through a series of ethanol and acetone solutions, and embedded in Epon 812 (Roth). Ultrathin sections were cut, stained with uranyl acetate/lead citrate (Fluka) and examined with a JEM-100CX (JEOL) transmission electron microscope.

Statistical analysis

The analysis was performed using statistical software packages (StatSoft, Tulsa, OK; GraphPad Prism, San Diego, CA). The data obtained were compared by the non-parametric Mann–Whitney *U* or the Duncan's test (for more than ten repeats). Statistical significance was determined at the level of $P < 0.05$, unless otherwise indicated.

Results

Analysis of selected markers of senescence and cell death in A549 cells after treatment with doxorubicin

To determine the extent of senescence/cell death induced by doxorubincin in the A549 cell population, we studied some features potentially related to the execution of these programs, such as SA β-galactosidase expression, DNA fragmentation, phosphatidylserine externalization and cell membranes integrity. Moreover, we examined cell morphology by TEM and cell cycle progression in control cells and cells subjected to the treatment.

The range of doses used in these experiments was established primarily on the basis of their ability to enhance the activity of SA β-galactosidase. The cells were cultured in the presence of gradually increasing concentrations of the cytostatic (10, 25, 35, 50, 70, 100, and 200 nM), and assayed for the activity of this enzyme at day 4 after the treatment has begun. Statistical data showed that there was a significant increase in the mean percentage of cells displaying elevated SA β-galactosidase activity at all

indicated doses, compared to control cells (ANOVA; Duncan's test, $P < 0.05$). However, only those concentrations that resulted in very highly significant differences compared to control cells ($P < 0.001$) and, at the same time, revealing significant differences among one another ($P < 0.05$), i.e., 50, 100 and 200 nM, were chosen for further studies (Figs. 1, 2).

Since it has been reported that cell cycle arrest at the G_0/G_1 or G_2/M boundaries, as well as cytokinetic block, may be indicative of senescence-like alterations and followed by cell death events, we analyzed cell cycle distribution in A549 cells in our experimental conditions. As regards the G_0/G_1 and S phases of the cycle, there was a statistically significant decrease in the median percentage of cells with DNA content corresponding to these phases after treatment with all the concentrations used, in comparison with the population of control cells (non-parametric Mann–Whitney U statistics, $P < 0.05$) (Figs. 3, 4). Concurrently, a significant increase in the median percentage of cells classified as G_2/M, according to their DNA content, has been observed as a consequence of exposure to all doses of doxorubicin. Nevertheless, such an accumulation of cells in G_2/M compartment did not reflect a straightforward tendency, because the median percentage of cells was lower at the dose of 200 nM than at 50 or 100 nM in this case (Fig. 4). On the other hand, a quantitative estimation of cells with more than 4n DNA content revealed that the rate

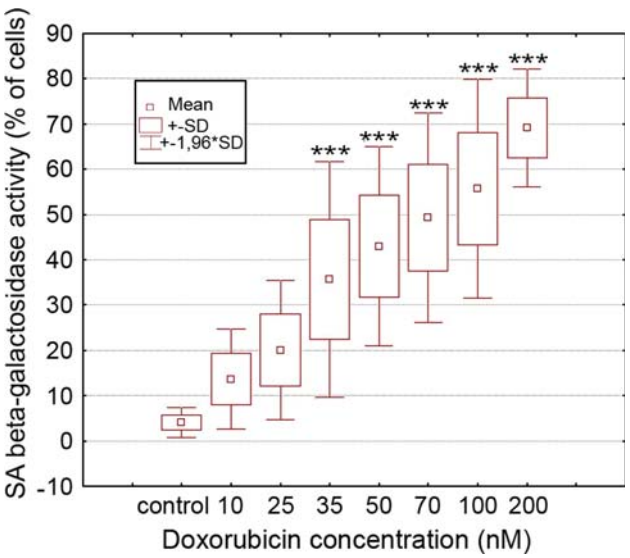

Fig. 1 Activity of senescence-associated β-galactosidase in A549 cells after treatment with doxorubicin. A549 cells were exposed to indicated concentrations of the drug for 72 h, incubated in drug-free medium for further 24 h and assayed for the activity of the enzyme at pH 6. Results corresponding to very highly statistically significant differences ($P < 0.001$) as compared with control cells are marked with *asterisks*. Data are representative of ten independent experiments

of polyploidy on the cell population level appeared to be dose-dependent, with significant differences for all doxorubicin concentrations tested in comparison with control cells (Fig. 4). Similarly, an increased number of cells with the $subG_1$ characteristics typical of fractional, presumably apoptotic DNA content, was detected, but only at 100 and 200 nM doxorubicin (Figs. 3, 4).

To further verify these observations and to resolve the question if the above-described fluctuations in the percentages of cells between cell cycle phases were related to G_2/M arrest, or rather to an elevated rate of cell death in G_0/G_1 and S phases, resulting from DNA fragmentation after treatment, we performed the TUNEL assay. The data obtained by this method confirmed that the maximal level of cell death was induced in cells incubated with the highest concentrations of the cytostatic (Figs. 5, 6). Moreover, the number of TUNEL-positive cells reached a peak at the dose of 200 nM, exceeding 52% of the cell population. As opposed to cells with $subG_1$ DNA content, the increase in the median percentage of cells incorporating dUTP-FITC into their DNA was evident even at the lowest dose used in our experiment (Figs. 5, 6). According to the results of bivariate analysis of dUTP-FITC positive cells versus DNA content, it does not seem probable that cells in G_0/G_1 or S phases would be more susceptible to cell death than cells in G_2/M (Fig. 7). On the contrary, the cells with DNA content corresponding to G_2/M phases and especially polyploid cells constituted a predominant fraction of TUNEL-positive cells in the whole cell population. Thus, the cells from G_0/G_1 and S phases of the cell cycle may have been accumulated at G_2/M or even may have entered polyploidy to some extent. Analogically, since the cells in G_2/M does not seem to have considerably more damages in their DNA than the polyploid population (Fig. 7), but, at the same time, there is a statistically significant decrease in G_2/M population and increase in the percentage of cells with more than 4n DNA content at 200 nM as compared to 100 nM doxorubicin, it is highly probable that some of the cells from G_2/M became polyploid. Bearing in mind that the increased percentage of cells in G_2/M after the treatment compared to the control cells did not follow a clear tendency, like polyploidy did, we suggest that the most prominent accumulation of cells in G_2/M occurring at 50 and 100 nM may reflect an emerging cell cycle arrest typical of a senescence-like state, which was at least partly transient, followed by polyploidization and cell death, especially at 200 nM of the drug. There was, however, still a relatively small percentage of the cells arrested as compared to the percentage of the cells with elevated SA β-galactosidase expression, indicating that senescence induced in these conditions may not be a stable, permanent program, at least at this time point. In order to discriminate at which doses of doxorubicin DNA fragmentation

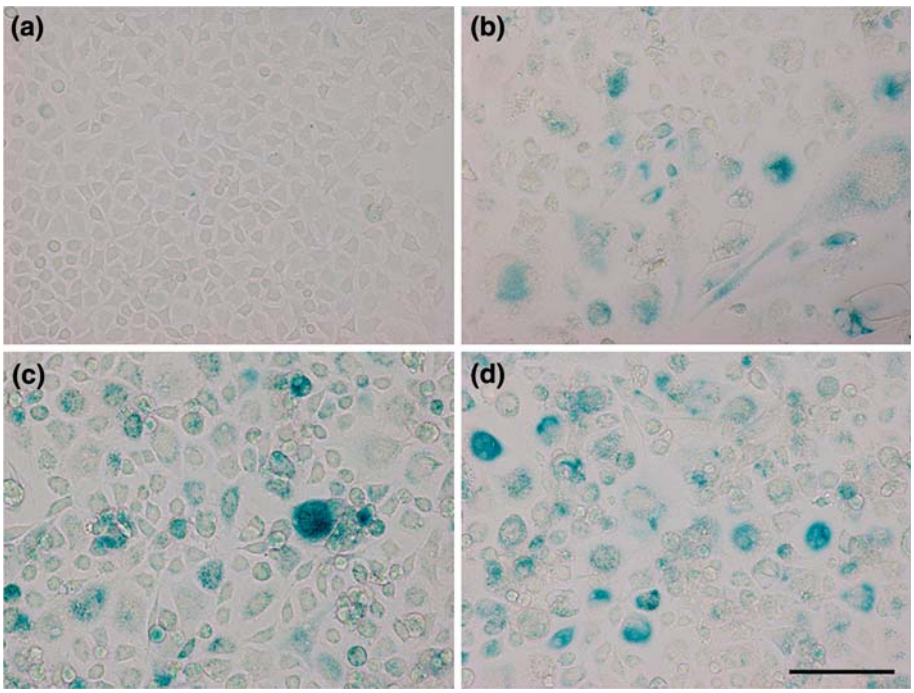

Fig. 2 Activity of senescence-associated β-galactosidase in A549 cells after treatment with doxorubicin—light microscopic examination. **a** Control, **b** 50 nM of doxorubicin, **c** 100 nM of doxorubicin, and **d** 200 nM of doxorubicin. Visible changes in cell morphology. Results are representative of ten independent experiments (*bar* 100 μm)

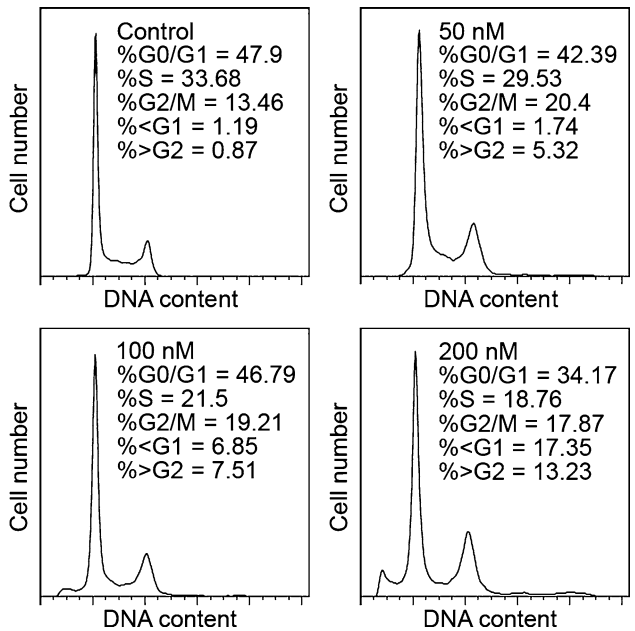

Fig. 3 Flow cytometric examination of the cell cycle distribution of A549 cells—staining with RNase/PI. Representative *histograms* are shown: *upper left* control, *upper right* 50 nM of doxorubicin, *lower left* 100 nM of doxorubicin, and *lower right* 200 nM of doxorubicin. According to DNA content, the following categories were distinguished: cells with DNA content corresponding to G_0/G_1, S and G_2/M phases, as well as cells with fractional subG_1 and polyploid DNA content

revealed by the TUNEL technique was in fact related to senescence/cell death and how it was reflected by chromatin condensation at the ultrastructure level, we further studied phosphatidylserine externalization and cell membranes integrity in the annexin V/PI assay and we analyzed cell morphology by TEM.

As compared with the TUNEL method, the annexin V/PI staining showed similar tendency, but the lower extent of cell death in the A549 cell population or, alternatively, was less sensitive in our experimental conditions. Treatment with all the concentrations of doxorubicin resulted in a statistically significant increase in the number of early apoptotic, late apoptotic and necrotic cells (Fig. 8). At 200 nM doxorubicin, the median values for annexin V-positive/PI-negative (early apoptotic), annexin V-positive/PI-positive (late apoptotic), annexin V-negative/PI-positive (necrotic) cells were 7.9, 3.1 and 7.6%, respectively. The appropriate percentages for the two other doses, 50 and 100 nM doxorubicin, were markedly lower (Fig. 8), but at the same time did not differ significantly from each other at these concentrations. Irrespective of the method employed, the highest drug concentration had undoubtedly the most prominent effect as regards cell death induction.

Our observations by TEM confirmed that in the A549 cell population following doxorubicin treatment a sequence of changes occurred, manifesting itself in a gradual progression to cells increased in size, displaying enhanced cytoplasmic granularity and vacuolization, rich in myelin-like structures, with segmented nuclei often containing condensed chromatin and with rather well-preserved other organelles, especially a relatively large amount of mitochondria and few autophagic vacuoles (Fig. 9). These alterations, probably indicative of a senescence-like state resulting from DNA damage and oxidative stress, might be

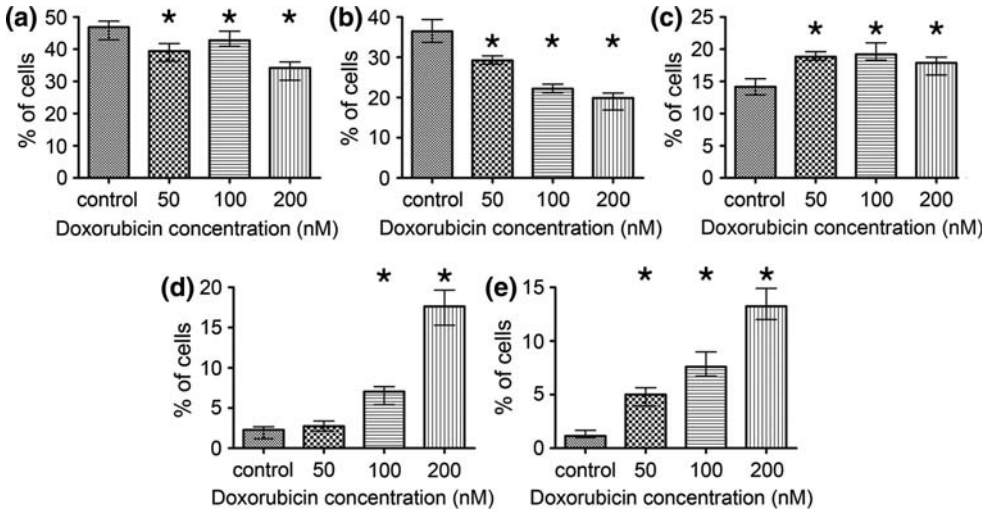

Fig. 4 **a**–**e** Flow cytometric examination of the cell cycle distribution of A549 cells—staining with RNase/PI. *Diagrams* for each of the groups defined according to DNA content are shown. **a** Cells with DNA content corresponding to G_0/G_1 phases, **b** cells with DNA content corresponding to S phase, **c** cells with DNA content corresponding to G_2/M phases, **d** cells with DNA content corresponding to $subG_1$ fraction, and **e** cells with DNA content corresponding to polyploidy. *Columns* median percentage of cells and *bars* interquartile range. Statistically significantly different results ($P < 0.05$) as compared with control cells are marked with *asterisks*. Results are representative of five independent experiments

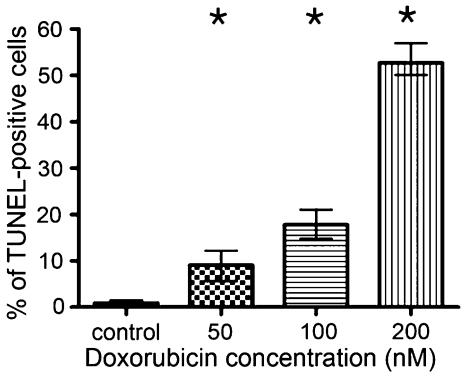

Fig. 5 Flow cytometric examination of DNA fragmentation—the TUNEL method. *Columns* median percentage of TUNEL-positive cells and *bars* interquartile range. Statistically significantly different results ($P < 0.05$) as compared with control cells are marked with *asterisks*. Results are representative of five independent experiments

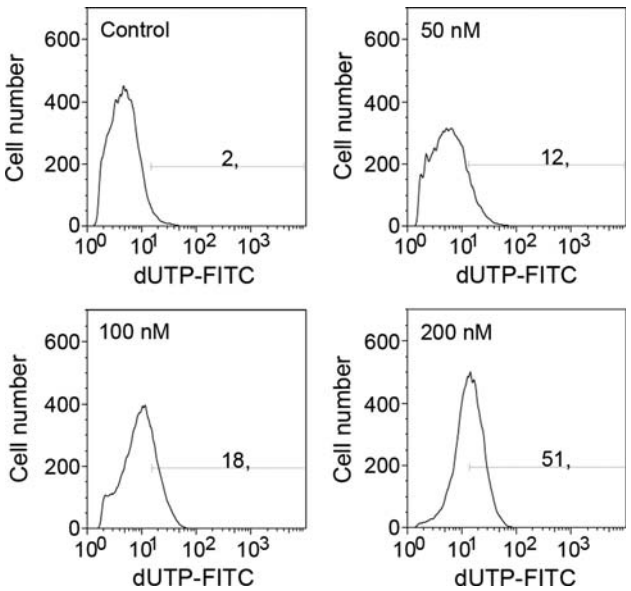

Fig. 6 Flow cytometric examination of DNA fragmentation—the TUNEL method. Representative *histograms* are shown: *upper left* control, *upper right* 50 nM of doxorubicin, *lower left* 100 nM of doxorubicin, and *lower right* 200 nM of doxorubicin. The percentage of TUNEL-positive cells is given on the *horizontal line*

followed by a greater incidence of aberrant mitoses, which in turn lead to multinucleation during mitotic catastrophe. Indeed, cells with multiple nuclei were present, especially at 100 and 200 nM doxorubicin (Fig. 9). Eventually, at the highest concentration of the drug, some cells showed morphological features of cell death, like densely condensed chromatin, more prominent vacuolization and loss of intact, easily recognizable organelles, typical of late apoptosis or rather secondary necrosis (Fig. 9). Nevertheless, this heterogeneous cancer cell population still contained a certain number of cells, which did not appear to follow this route, and as such they may contribute to chemotherapeutic resistance.

Vimentin cytoskeleton

As an intermediate protein, vimentin is believed to be differently regulated during senescence/cell death events, and is involved in epithelial-to-mesenchymal transition during tumor progression, we aimed at identifying possible

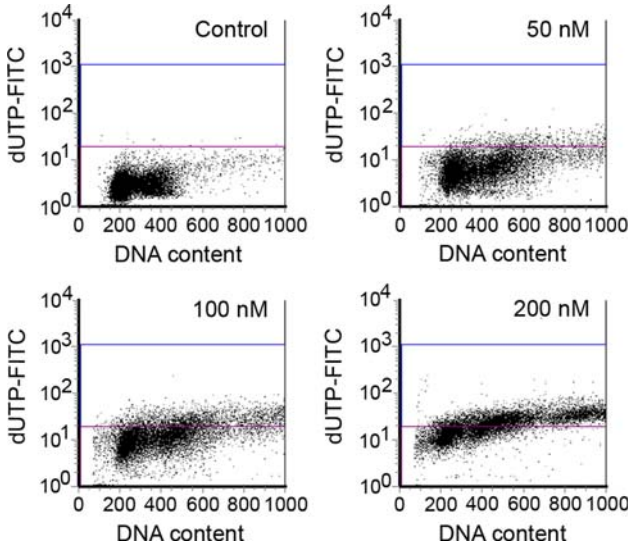

Fig. 7 Flow cytomertic examination of DNA fragmentation in relation to DNA content. Representative *dot-plots* are shown: *upper left* control, *upper right* 50 nM of doxorubicin, *lower left* 100 nM of doxorubicin, and *lower right* 200 nM of doxorubicin

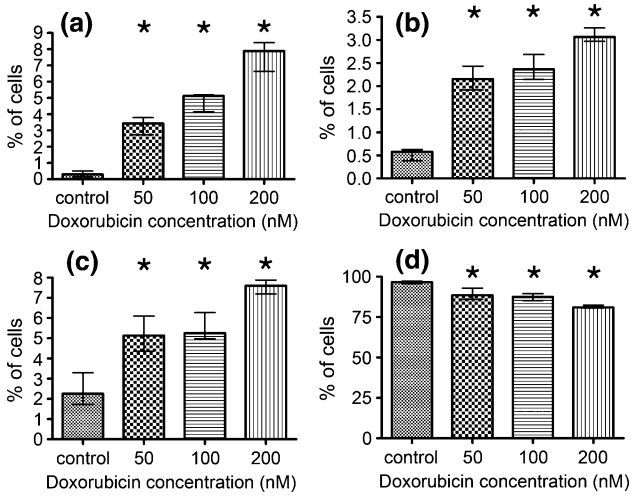

Fig. 8 Flow cytometric examination of apoptosis, necrosis and cell viability—the Annexin V/PI assay. *Diagrams* show four subgroups of cells. **a** Early apoptotic: annexin V+, PI−. **b** Late apoptotic: annexin V+, PI+. **c** Necrotic: annexin V−, PI+. **d** Viable: annexin V−, PI−. *Columns* median percentage of cells and *bars* interquartile range. Statistically significantly different results ($P < 0.05$) as compared with control cells are marked with *asterisks*. Results are representative of five independent experiments

changes in the organization and/or the level of vimentin in A549 cells exposed to doxorubicin.

Flow cytometric examination revealed that the median percentage of vimentin-positive cells remained markedly unchanged for all the doses used as compared with the control cells, falling within the range of 93–96% for each experimental condition (Fig. 10). Hence, it was possible to exclude that any difference in fluorescence intensity would have been over- or underestimated due to uneven antibody distribution during staining procedure. As regard the second analyzed parameter, i.e., the mean fluorescence intensity, which fitted well with an intracellular level of vimentin, we noted some alterations. After an initial, slight and statistically insignificant increase at the dose of 50 nM, the median value of this parameter reached a statistically justified maximum at 100 nM doxorubicin, and finally decreased to a slightly elevated, but statistically insignificant level at the highest dose as compared to the control cells (Fig. 11). To determine the effect of doxorubicin on the vimentin cytoskeleton, morphology and arrangement of this type of intermediate filaments were visualized by fluorescence microscopy. In the untreated cell population, the vimentin network was subtle, relatively well organized, mainly composed of thin and short filaments uniformly distributed throughout the cytoplasm and typical foci in the perinuclear region (Fig. 12). While the shape and the volume of cells changed after the treatment, a considerable heterogeneity in appearance and cytoplasmic location of filaments occurred as well (Fig. 12). At the lowest drug dose, apart from markedly unchanged cells, those with increased volume were observed, which contained dense thick bundles running not only along the main axis of the cell, but also around the nucleus. These cells seemed to be more abundant at 100 nM doxorubicin. Long and well-spread filaments reached the peripheral regions of cells, but simultaneously few less-regularly arranged and dispersed fibers may have been observed in the vimentin network. It is possible, perhaps, that accumulating vacuoles and inclusions were anchored to the cytoskeleton of senescent cells in these areas. Additionally, a population of multinucleated cells grew in number at this concentration, with the vimentin cytoskeleton retracted around nuclei in the form of compact rings and progressively disorganized peripheral network. These features were also evident at the highest drug dose (Fig. 12). Besides that, in part of cells from this population, the normal network became somewhat less visible and often disappeared, resulting in diffuse, but sometimes intense fluorescent staining of aggregates and more amorphous structures, what could possibly have reflected cleavage and subsequent collapse of vimentin into the nucleus (Fig. 12).

G-actin cytoskeleton

For evaluation of possible changes in localization and nuclear content of G-actin during senescence/cell death events, we performed fluorescence microscopic examinations of A549 cells after treatment with doxorubicin. The organization of this protein was analyzed using two known probes for G-actin detection in fixed cells: vitamin D-binding protein (VDBP) and deoxyribonuclease I (DNase

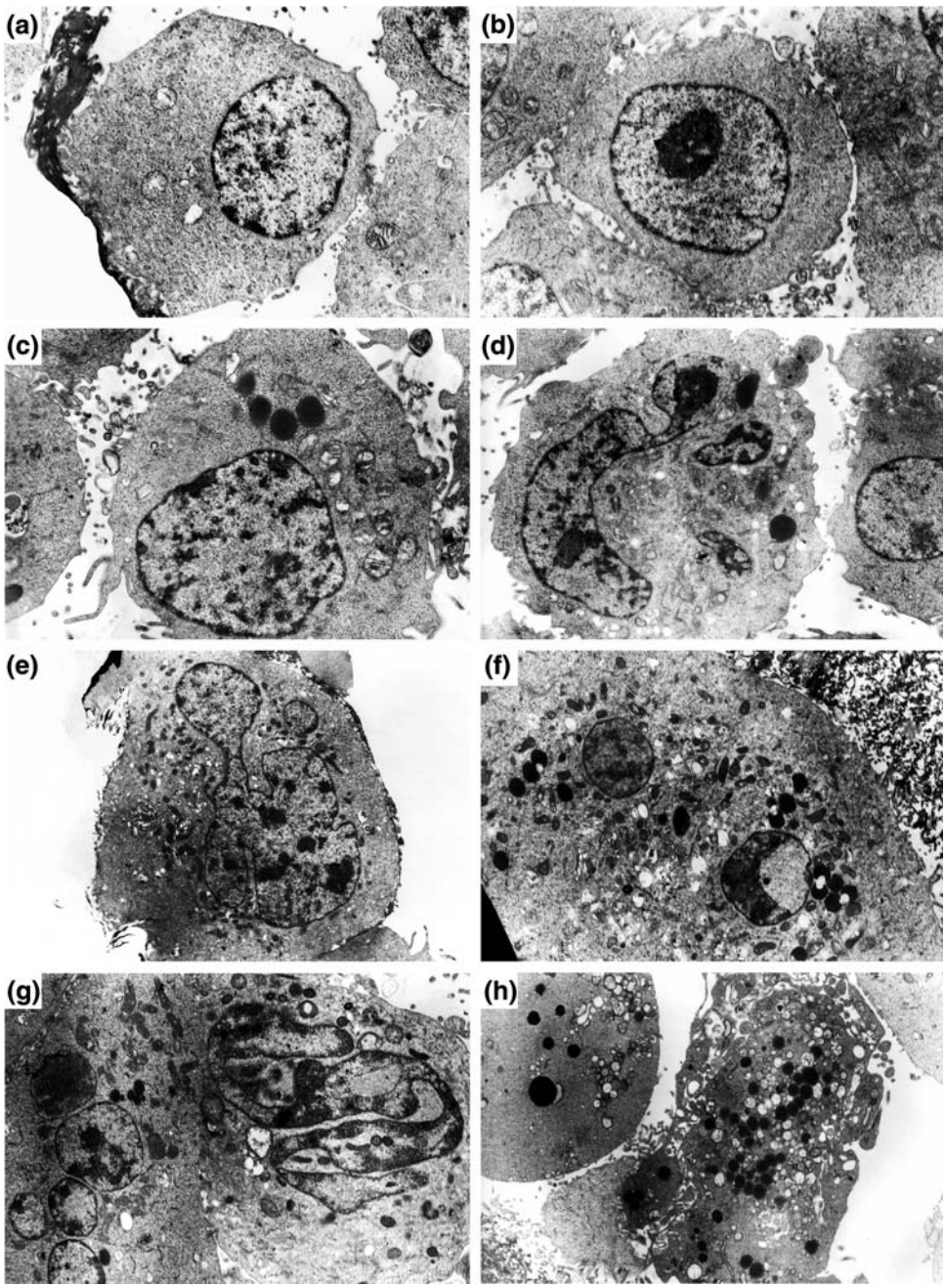

Fig. 9 Electron microscopic examination—cell morphology. **a**, **b** Controls (×4,700), **c**, **d** 50 nM of doxorubicin (×4,500), **e**, **f** 100 nM of doxorubicin (×2,400 and ×3,000, respectively), **g** low and right, and **h** 200 nM of doxorubicin (×3,000). Progressive alterations of the nucleus and cytoplasm are visible in doxorubicin-exposed cells. Results are representative of five independent experiments

I). As regards both procedures, G-actin seemed to be more concentrated at the perinuclear area and/or possibly in the nucleus after treatment with doxorubicin, what was visible in some of the enlarged cells or in some of those with segmented/multinucleated nuclei (Fig. 13). This structures around some nuclei were arranged similarly to those ring-like observed in vimentin staining, but gave weaker, delicate, mostly diffuse fluorescent signal. We also observed some foci, among them few dot-like structures, which were localized in the peripheral, cortical or central regions of the cytoplasm and might have been involved in the nucleation of actin filaments. Apart from that, a very bright fluorescent signal was detected around pyknotic nuclei or those with signs of karyorrhexis, especially with chromatin dispersed into apoptotic bodies in both methods used (Fig. 13). At the same time, G-actin appeared to be more evenly distributed in the control cells, except from dividing ones (Fig. 13). According to our observations, DNase I, apart from its high affinity to G-actin, may potentially bind to DNA as well. Therefore, for quantitative measurements in the nucleus area, the cells were stained with a more accurate probe in these conditions, i.e., VDBP. In our experiment, the median fluorescence intensity of G-actin in the nucleus defined as a mean grey value seemed to be

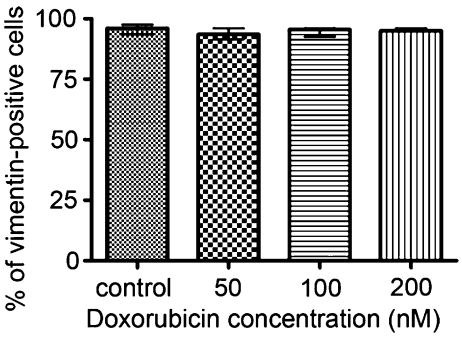

Fig. 10 Flow cytometric examination—the percentage of vimentin-positive cells in the population. *Columns* median percentage of vimentin-positive cells and *bars* interquartile range. Statistically significant differences as compared to control cells were not observed. Results are representative of five independent experiments

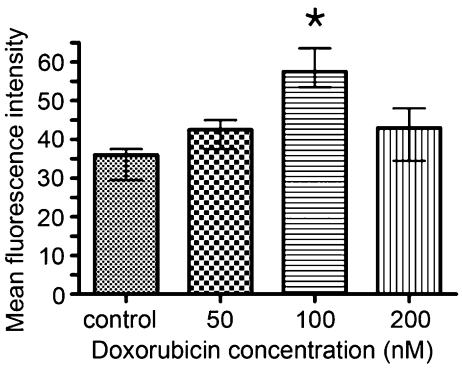

Fig. 11 Flow cytometric examination—fluorescence intensity of vimentin (reflecting vimentin content) expressed as a geometric mean. *Columns* median fluorescence intensity and *bars* interquartile range. Statistically significantly different results ($P < 0.05$) as compared with control cells are marked with *asterisks*. Results are representative of five independent experiments

slightly increased only at 50 and 100 nM doxorubicin as compared with the control cells (Fig. 14). However, the mean grey values corresponding to the doxorubicin concentrations used in this study did not differ statistically either from control values or from one another. At the same time, there were not statistically significant changes in fluorescence intensity between the negative control cells exposed to doxorubicin and the untreated population of negative control cells (Fig. 15).

Discussion

Not only cell death, but also senescence on the cellular level may function as a fail-safe tumor-suppressor mechanism. Hence, it seems that, for the evaluation of chemotherapeutic effectiveness, both forms of cellular response should be taken into account. Resistance to cell death, but also escape from senescence could be crucial for malignant transformation and contributes to the failure of chemotherapy (Rebbaa 2005). In this study, we treated the human non-small cell lung carcinoma A549 cells with increasing concentrations of doxorubicin in order to induce these different phenomena and to observe associated changes of the cytoskeleton.

SA β-galactosidase was first described in keratinocytes and fibroblasts as a senescence marker, which was absent from presenescent, quiescent, terminally differentiated and immortal cells. On the other hand, manipulations resulting in senescence of immortal cells were also related to SA β-galactosidase induction (Dimri et al. 1995). Therefore, an enhanced activity of this enzyme has been broadly used for identification of senescent cells in vitro and in vivo, including cancer cells after treatment (van der Loo et al. 1998; Mishima et al. 1999; Chang et al. 2002; Schmitt et al. 2002; te Poele et al. 2002; Douarre et al. 2005; Klein et al. 2005; Arthur et al. 2007; Feldser and Greider 2007). Although the optimal activity of lysosomal β-galactosidase was revealed at pH 4, it has been shown that the threshold level, at which mostly senescent cells were detected, was at pH 6. Due to the increased lysosomal content and changed lysosomal functions, the activity of this enzyme is most probably elevated in senescence to such an extent that it becomes detectable at suboptimal pH 6 and, in this situation, it reflects altered cellular metabolism (Dimri et al. 1995; van der Loo et al. 1998; Kurz et al. 2000; Lee et al. 2006). Consistently, in our study, not only SA β-galactosidase activity was elevated in the A549 cells exposed to doxorubicin, but also there appeared more abundant and larger lysosomes on the ultrastructural level, which probably accumulated non-degradable materials, such as lipofuscin and/or organelles. Since an increase in lysosomal mass may be indicative of autophagy as well, as evidenced by acridine orange staining (Arthur et al. 2007), it seems that SA β-galactosidase activity could additionally reflect this form of cell death. In our experiment, however, externalization of phosphatidylserine, which is a common event in apoptotic and autophagic cell death (Lockshin and Zakeri 2004), was relatively low and reached the maximum median value, i.e., 10.95% of the cellular population for the highest dose of doxorubicin. Concurrently, the majority of cells (almost 70%) were positive for an increased level of SA β-galactosidase. Nevertheless, because the activity of this enzyme could potentially be enhanced in other than senescence conditions related to an increased lysosomal content, evaluation of different senescence-associated symptoms would also be advisable for proper determination of senescence (Kurz et al. 2000; Lee et al. 2006).

In agreement with that, in our study, other senescence features, apart from SA β-galactosidase activity, were evaluated, i.e., cell cycle disturbances, chromatin condensation, increased cytoplasmic granularity and cell volume,

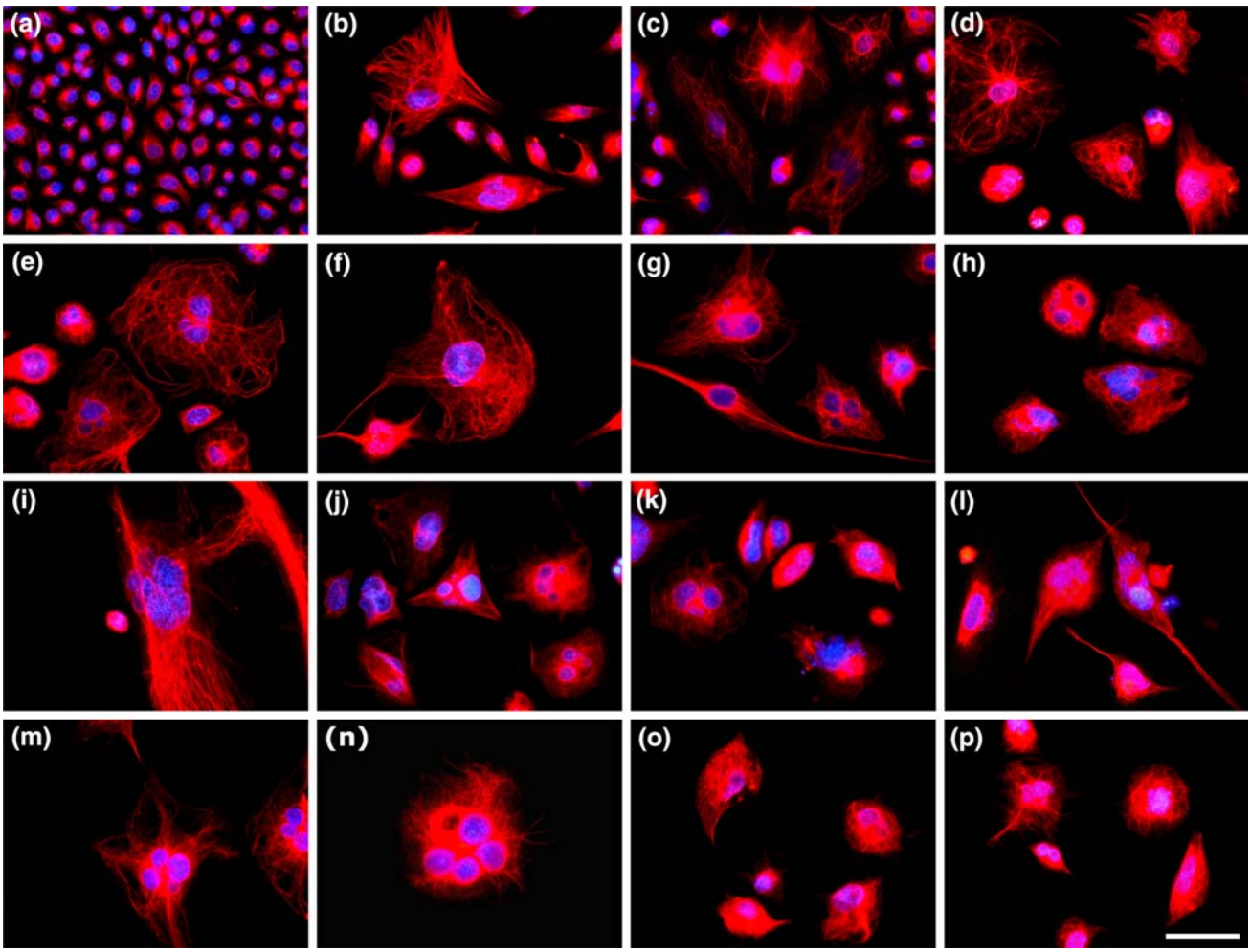

Fig. 12 Fluorescence microscopic examination—organization of vimentin. A549 cells were incubated with increasing concentrations of doxorubicin and stained for the presence of vimentin. **a** Control, **b–d** 50 nM, **e–h** 100 nM, and **i–p** 200 nM. Visible heterogeneity of vimentin organization: thin, but well-organized filaments in control cells; dense, thick bundles and well-spread filaments in senescent-like cells; more contracted cytoskeleton and compact rings around nuclei in multinucleated cells; diffuse fluorescent signal around nuclei with features of karyorrhexis or karyolysis in dying cells. Nuclei were counterstained with DAPI. Results are representative of five independent experiments (*bar* 50 μm)

polyploidy, as well as relatively low cell death rate and, finally, some specific changes in the cytoskeleton. Senescence of A549 cells after treatment with doxorubicin was previously reported (Crescenzi et al. 2005; Klein et al. 2005). Similar extent of senescence measured by SA β-galactosidase activity was documented in our work, with minor differences most probably resulting from different experimental conditions and/or functional changes in senescent lysosomes. Some authors even considered that this phenomenon induced by doxorubicin in A549 cells could serve as a model of potent senescence induction for further comparisons (Klein et al. 2005). SA β-galactosidase seems to be neither responsible for cell cycle arrest during senescence nor required for senescence per se (Dimri et al. 1995; Lee et al. 2006). Therefore, an uncoupling between activity of this enzyme and cell cycle arrest is possible, what may be supported by our results as well. Namely, we detected relatively high SA β-galactosidase expression; more than 55% of the cells at 100 nM doxorubicin, but only about 4% of the control cells revealed its enzymatic activity, whereas the median percentage of cells with DNA content corresponding to G_2/M was only 19.2 at this dose, and 14.2 for the control cells. Due to increased polyploidy resulting from the exposure to doxorubicin, we cannot discount the possibility that some cells with G_2/M DNA content are actually G_1 tetraploid cells. Moreover, although SA β-galactosidase activity increased further at 200 nM as compared with 100 nM, a decrease in the median percentage of G_2/M cells appeared concomitantly. At the same time, the cells with DNA content corresponding to G_0/G_1 did not seem to be arrested as compared to control cells, because their percentage decreased, and a comparison of

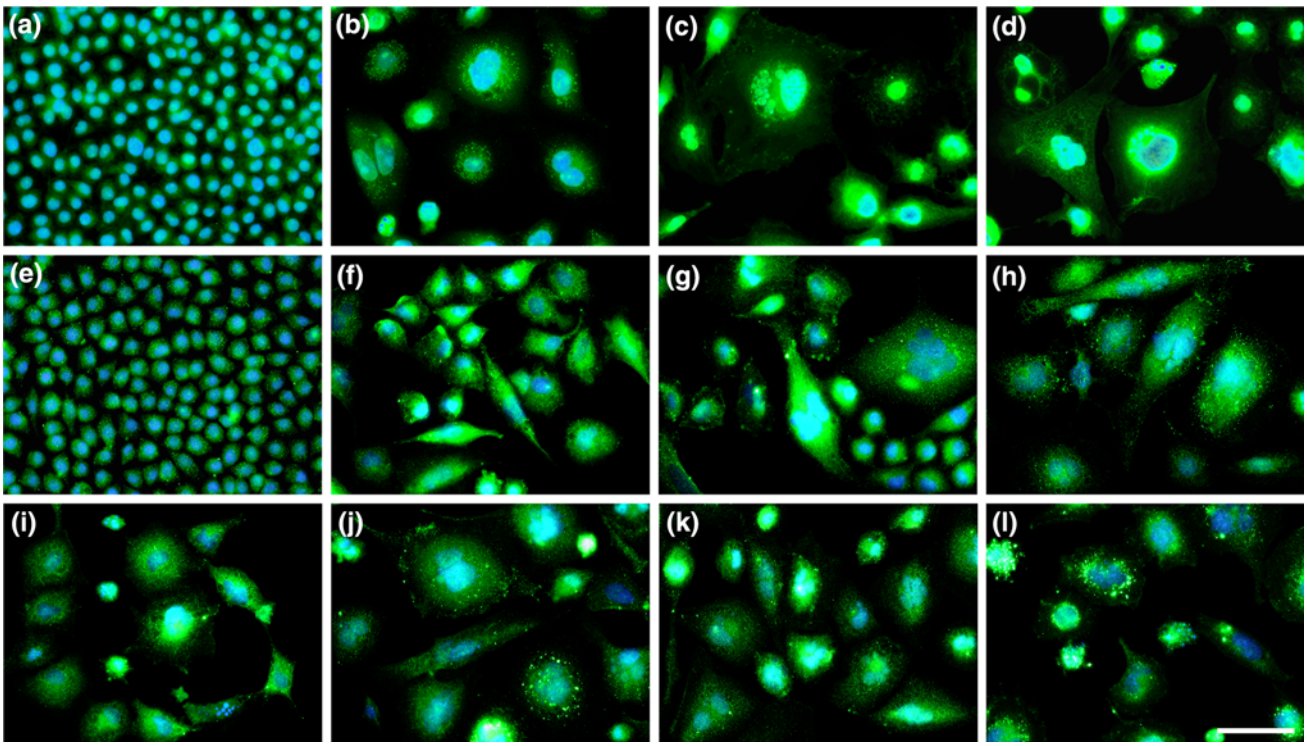

Fig. 13 Fluorescence microscopic examination—organization of G-actin. A549 cells were incubated with increasing concentrations of doxorubicin and stained for the presence of G-actin using two known probes for this protein, i.e., DNase I: **a** control, **b** 50 nM, **c** 100 nM, **d** 200 nM and VDBP: **e** control, **f**, **g** 50 nM, **h**, **i** 100 nM, **j**–**l** 200 nM. G-actin concentrates in the perinuclear region of some cells after treatment. Visible also *dot-like* structures in the cytoplasm and a very bright, intense fluorescent signal in cells containing apoptotic bodies. Nuclei were counterstained with DAPI. Results are representative of five independent experiments (*bar* 50 μm)

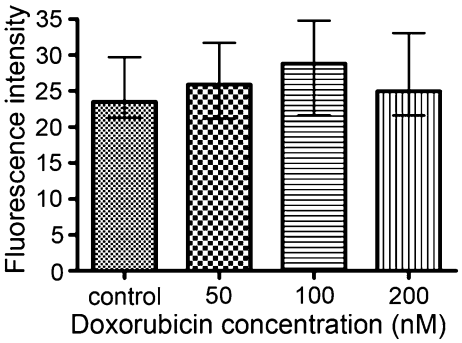

Fig. 14 Quantitative fluorescence assay—fluorescence intensity of G-actin (reflecting G-actin content) expressed as mean grey value, in isolated nuclei of A549 cells. *Columns* median fluorescence intensity and *bars* interquartile range. Only slight fluctuations were observed, without statistically significant differences in comparison with control cells. Results are representative of five independent experiments

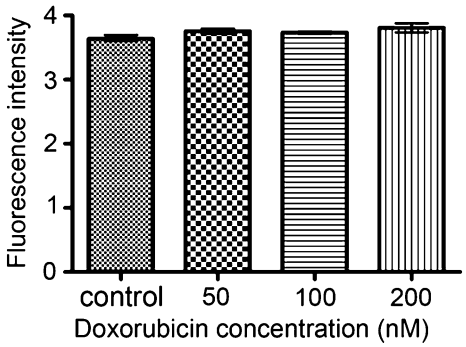

Fig. 15 Quantitative fluorescence assay—fluorescence intensity of nuclei isolated from negative control A549 cells (mean grey). Cells were stained as for detection of G-actin, but, instead of primary antibody, a specific blocking peptide was used (Santa Cruz Biotechnology). *Columns* median fluorescence intensity and *bars* interquartile range. Statistically significant differences as compared to control cells were not observed. Results are representative of five independent experiments

the subsequent doses revealed only an insignificant, 3%, increase in this population at 100 nM doxorubicin, followed by a significant decrease at 200 nM. One possible explanation might be the instability of the induced program, i.e., the fact that most of the cells with elevated SA β-galactosidase expression were unable to arrest permanently so that they progress through subsequent phases of the cell cycle. A similar discrepancy between a senescence-like phenotype and cell cycle block was reported in human diploid fibroblasts transfected with HPV *E6* oncogene that maintained decreased levels of $p21^{Cip1/Waf1/Sdi1}$ through p53 degradation and in $p21^{Cip1/Waf1/Sdi1}$ nullizygous mouse embryonic fibroblasts (Dulić et al. 2000). Katakura et al.

(1999) proposed that the execution of premature senescence features and growth arrest were differently controlled in TGF-β-treated A549 cells, with impaired molecules responsible for the latter function. As opposed to that, somewhat more visible accumulation of A549 cells in G_2/M after treatment with doxorubicin was reported by Crescenzi et al. (2005), presumably as a consequence of the longer recovery-time. Alternatively, extended periods of treatment also resulted in the more prominent cell cycle block in G_2 and, probably, G_1 (Klein et al. 2005). At present, we cannot therefore exclude that a longer period of treatment or time without doxorubicin, associated with activation of more tumor-suppressor genes with different complementary functions, would have been crucial for the full-blown senescence program related to a more pronounced cell cycle arrest. $p21^{Cip1/Waf1/Sdi1}$ protein is believed to be involved in an initial stage of senescence execution and cell cycle arrest, whereas, following its decline, $p16^{Ink4a}$ accumulates in order to keep the senescence program stable (Stein et al. 1999; Dulić et al. 2000). It was suggested that in A549 *p16*^{Ink4a}-deleted cell line, functions of the lacking protein might be substituted by $p21^{Cip1/Waf1/Sdi1}$ (Klein et al. 2005), but it is unclear at the moment if and how such a deficiency may have impaired cell cycle block in our experiment. Indeed, $p21^{Cip1/Waf1/Sdi1}$ was shown to be up-regulated in doxorubicin-treated A549 cells (Crescenzi et al. 2005). On the other hand, however, inactivation of *p16*^{Ink4a} delays the execution of senescence in human fibroblasts (Brookes et al. 2004). $p16^{Ink4a}$ contributes to G_1 cell cycle arrest in the consequence of pRb hypophosphorylation. It was even hypothesized that only *p21*$^{Cip1/Waf1/Sdi1}$, transcriptionally activated by p53 in response to DNA damage, without $p16^{Ink4a}$ activity, may not be sufficient for irreversibility of the senescence-associated cell cycle arrest in certain conditions (Stein et al. 1999; Beauséjour et al. 2003). Moreover, the senescence program in A549 cells may be substantially compromised as a result of deletion of the *Ink4b/Arf/Ink4a* locus (Okamoto et al. 1995; Xie et al. 2005). Since this locus, apart from *p15*^{Ink4b} and *p16*^{Ink4a}, contains also *p14*^{Arf}, its mutations interfere with the two major tumor-suppressor pathways, i.e., via pRb and p53. To activate $p21^{Cip1/Waf1/Sdi1}$-mediated senescence in this situation, p53 must be stabilized by factors independent of $p14^{Arf}$ (Ashcroft and Vousden 1999). Nevertheless, deletion of *p14*^{Arf} may diminish p53-mediated induction of *p21*$^{Cip1/Waf1/Sdi1}$ (Kamijo et al. 1997). In fact, the results obtained by us (data not shown) and others (Klein et al. 2005) indicate that a considerable part of the A549 population was able to restore its proliferative capacity after few additional days in culture. What is more, DNA topoisomerase inhibitors were shown to be efficient but reversible inducers of premature senescence in human fibroblasts (Michishita et al. 1998). In this work, we observed that only part of SA β-galactosidase expressing cells may have been arrested, but alternatively, after release from G_2/M block, some of them might have undergone endoreduplication (Arthur et al. 2007; Walen 2007) and/or might have died by delayed mechanisms, e.g., as a consequence of abortive mitosis. Accordingly, it has been previously shown that doxorubicin is able to induce features of both senescence-like response and mitotic catastrophe in A549 and Huh-7 cells, which might, in turn, further contribute to stress-induced premature senescence and likely ends up with cell death (Eom et al. 2005; Klein et al. 2005). Besides that, some proliferating cells might have still been arrested even beyond the G_2 checkpoint and the mitotic spindle checkpoint, i.e., at cytokinesis (Dulić et al. 2000). These suggestions are consistent with the presence of many cells with multiple nuclei after treatment with doxorubicin in our experiment.

In this study, a 100 nM concentration of doxorubicin appeared to be the most effective for inducing cell cycle arrest. Consistently with senescence execution, we also documented altered morphological features such as increased cell volume and granular cytoplasmic content, apparent chromatin condensation and heterogeneity in nuclear shape by electron microscopy. Polyploidy, indicative of senescent cell populations and observed in aging/late passage cells by others (Sherwood et al. 1988; Walen 2007; Yang et al. 2007), rose in A549 cells after incubation with doxorubicin as well.

Furthermore, a relatively low rate of cell death was detected by the Annexin V/PI assay and analysis of the $subG_1$ fraction in comparison with the TUNEL assay in our experimental conditions. We suppose that such a result might be related to the mode of action of doxorubicin, i.e., DNA damage. Apart from cells actually suffering from apoptotic and necrotic cell deaths, some cells with non-lethal, reparable lesions could possibly be detected by dUTP incorporation. As regards induction of cell death measured by the Annexin V/PI assay, the most visible difference was observed between the cells exposed to either 50 or 100 and 200 nM doxorubicin. On the contrary, the median percentages of early apoptotic, late apoptotic and necrotic cells did not seem to change significantly between the doses of 50 and 100 nM. Such an increase in the extent of cell death at 200 nM doxorubicin might be partly responsible for decreased G_2/M arrest at this concentration. Indeed, as the TUNEL results indicated, mostly cells with G_2/M DNA content and polyploid cells were affected by DNA double- or single-strand breaks at the highest dose of the drug. Previous studies have similarly documented rather low efficiency of cell death induction in the population of doxorubicin-treated A549 cells (He et al. 2005; Crescenzi et al. 2005; Filyak et al. 2007). Recently, a stem cell subpopulation has been isolated from A549 cell

line, displaying significantly lower Annexin V staining than the remaining cells in the presence of doxorubicin and as such probably contributing to resistance to this drug (Sung et al. 2008). Furthermore, senescent cells may be less susceptible to programmed cell death signals, e.g., those related to p53 induction, and, as a consequence of DNA damage, a substantial fraction of them die by necrosis (Seluanov et al. 2001), a phenomenon also evident in our experiment.

Along with elevated SA β-galactosidase activity, other phenotypic features of senescence and cell cycle disturbances, the moderate extent of cell death observed in our study was most probably indicative of the execution of a senescence-like state on the cellular level. The decrease in accumulation of cells at G_2/M visible at 200 nM might, in turn, reflect a shift toward more pronounced induction of cell death pathways, likely including mitotic catastrophe.

Constituents of the cytoskeleton belong to major protein components of the cell and some of them, like vimentin and actin, have been shown to participate in senescence, cell death and immortalization. Vimentin is ubiquitously present in cells of mesenchymal origin and thus is considered to be a marker of epithelial-to-mesenchymal transition, a process possibly associated with enhanced invasiveness and resistance of some cancers cells (Sommers et al. 1992; Thomson et al. 2005). Apart from that, increased vimentin expression and well-organized structure of vimentin filaments were demonstrated to be not only symptoms of replicative senescence, but also causative factors of morphological changes in senescent human fibroblasts (Nishio et al. 2001; Di Felice et al. 2005; Nishio and Inoue 2005). Our results seem to reveal some new aspects in this field like vimentin up-regulation and its organizational features in a stress-induced senescence-like state in cancer cells. The percentage of vimentin-positive cells did not change in the presented work, however, as evidenced by flow cytometric analysis, doxorubicin-treated A549 cells had higher levels of this protein than the control cells, but this difference was statistically significant only for 100 nM of the drug. Consequently, elevated levels of lethal stress at 200 nM might have been responsible for the decline in intracellular vimentin content and for the remodeling of intermediate filaments, observed in our experiment. Some reports have indeed documented that, as a substrate for caspases, vimentin was cleaved during early stages of apoptosis and, what is more, pro-apoptotic signals might be further reinforced by the product of this proteolysis (Byun et al. 2001; Nakanishi et al. 2001; Dinsdale et al. 2004). In fluorescence microscopic examination, we identified a quite heterogeneous organization of this cytoskeleton component, i.e., cells with well-developed and abundant filaments, cells with ring-like structures retracted around multiple nuclei and weaker peripheral signals and cells with diffuse staining probably resulting from vimentin collapse. Although the G_2/M arrest and vimentin levels show a similar general tendency after exposure to doxorubicin in this work, further studies are needed to establish if and how vimentin expression may be correlated with cell cycle regulation. Some suggestions appeared that vimentin is involved in cytoplasmic anchoring of p53 during senescence, which might contribute to limited rate of apoptosis (Nishio and Inoue 2005). If that would be the case, however, p53 would be unable to activate its transcriptional targets regulating cell cycle arrest, e.g., $p21^{Cip1/Waf1/Sdi1}$, and, consequently, tumor-suppressor mechanisms, including both cell death and senescence, would be impaired (Moll et al. 1996). The role of vimentin in senescence seems to be unclear at present. First, vimentin expression during this process may also be diminished (Moxham et al. 1998), because it rather depends on the cell or tissue type. Second, some authors propose its anti-oncogenic and suppressive function in cellular transformation, whereas the others indicate at its significance for senescence delay and spontaneous transformation (Nishio et al. 2001; Tolstonog et al. 2001). Since vimentin is thought to play a role in recombinational repair of nuclear and mitochondrial DNA (Tolstonog et al. 2001), it is therefore tempting to hypothesize that increased expression of this protein along with slight cell cycle disturbances and limited cell death during senescence-like state might reflect enhanced repair processes. But on the other hand, its permanent overexpression beyond a threshold level would promote recovery, senescence escape, genetic instability, immortalization and possibly support other adverse effects, as a potential mutator of the genome. Thus, although enhanced repair processes protect cells against replication of stress-induced mutations, they may also lead to the increased plasticity of the genome and invasiveness of cancer cells. Selective disruption of this cytoskeletal component in senescent cancer cells should therefore be considered as a target for cancer therapy. Actually, a mesenchymal–epithelial transition due to mutation of *Zeb1* transcription factor involves loss of vimentin expression and may lead to decreased proliferation and premature senescence (Liu et al. 2008).

In light of the above findings, it seems that, doxorubicin could have induced vimentin expression as a result of DNA damage and oxidative stress generation in our experiment. However, at higher concentrations of the drug, intracellular vimentin levels may have not been sufficient to cope with increasing DNA damage and p53 anchoring, probably contributing in this way to the activation of cell death pathways in some cells. At the same time, vimentin induction observed in our experiment was rather low as compared to the threefold higher levels in old cells in relation to those in young cells reported by Nishio et al. (2001).

The other cytoskeletal protein examined in our study was G-actin. In the nucleus area actin is believed to play an important role in chromatin remodeling, hence it may effect transcription, DNA cross-linking and chromosome morphology among the others (Olave et al. 2002). Since proper nuclear functions are affected in senescent/dying cells, as evidenced by cell cycle disturbances, DNA synthesis inhibition, mitotic abnormalities and profound changes in nuclear structure, it seems reasonable to hypothesize that all these features may be somehow influenced by nuclear actin. Therefore, in the current study, we analyzed the organization and nuclear level of G-actin in doxorubicin-treated A549 cells. It was previously reported that nuclear accumulation of actin along with enhanced expression and cytoplasmic localization of p-Erk1/2 as well as translocation of Rho family proteins occurs in replicative and premature senescence of human diploid fibroblasts. These results indicated that an impaired export of actin from the nucleus area due to dysregulated MEK signaling pathway may have been responsible for the changes observed (Lim et al. 2000). It was further supported by the findings that G-actin and cofilin accumulated in the nucleus of senescent cells. In aging fibroblasts arrested in G_1, cofilin was present in its active, dephosphorylated form that was able to sever F-actin (Kwak et al. 2004). Moreover, some suggestions exist that the level of nuclear actin may be somehow related to the proliferative capacity of the cell. In fact, forced nuclear export of actin not only reversed phenotypic and biochemical markers of senescence, but also stimulated replication, and, on the other hand, failure of actin export from the nucleus area resulted in growth arrest and senescent cell morphology (Wada et al. 1998; Kwak et al. 2004). In addition, G-actin in the nucleus was shown to be an early and universal marker of cellular senescence, suitable even for the detection of senescent cancer cells. Other authors also reported that cofilin-dependent nuclear import of actin may reflect cellular response to stress (Pendleton et al. 2003) and that similar stressor-induced changes may be controlled independently of apoptosis (Meijerman et al. 1999).

In our study, G-actin seemed to be more concentrated in the perinuclear/nuclear region of the cell after treatment with doxorubicin, as presumed from fluorescence intensity fluctuations. As revealed by quantitative fluorescence assay, its nuclear level changed only slightly after treatment, and that was substantiated by the lack of statistical significance. It is consistent with suggestions that dephosphorylated cofilin contributes to G-actin accumulation, because after treatment with doxorubicin we observed only a small G_2/M arrest, in which level of active cofilin seems to be the lowest as previously reported by Kwak et al. (2004). Since doxorubicin interferes with proper actin assembly dose-dependently (Colombo et al. 1988), one possible explanation of the slightly elevated level of nuclear G-actin in our study might be influence of this drug, and that was visible at 50 and 100 nM. Furthermore, oxidative stress, one of the modes of doxorubicin action, influences the amino acid sequence of G-actin and modifies the residues that are crucial for polymerization (Milzani et al. 2000). At the same time, levels of nuclear actin may be important for the modulation of BAF complexes, that are bound to actin (Rando et al. 2002), regulate activity of pRb tumor-suppressor (Dunaief et al. 1994) and as such effect not only G_1, but also G_2 cell cycle checkpoints. Besides that, nuclear G-actin controls activity of the transcription factor SRF, serum response factor, via the SFR cofactor MAL (Vartiainen et al. 2007).

As previously reported, F-actin was concentrated at the sites of apoptotic bodies formation (Grzanka et al. 2003), while in the current study we also found that G-actin was abundant in these regions, what implies that this protein may be involved in morphological signs of apoptosis. In agreement with these observations, G-actin acts as an inhibitor of DNase I, until it is proteolytically cleaved during apoptosis (Mashima et al. 1997; Eulitz and Mannherz 2007). At early stages of apoptosis, before cleavage of actin, down-regulation of its genes occurs, followed by accumulation of G-actin in apoptotic bodies (Guénal et al. 1997). These features along with a statistically insignificant decrease in G-actin content at the highest dose of doxorubicin in our study may reflect increasing cell death rate.

In conclusion, an uncoupling between phenotypic features of senescence and stable cell cycle arrest occurred in doxorubicin-treated A549 cells in our experimental conditions. It is in good accord with the genetic background of this cell line, i.e., the *Ink4b/Arf/Ink4a* locus deletion and might further imply one of the mechanisms of doxorubicin resistance.

Changes in the organization and level of G-actin were only slightly pronounced and insignificant, therefore its marked induction would not have been indicative of a transient senescent-like state, independent of G_1 cell cycle arrest. Changes in vimentin organization may have been related to morphological characteristics of senescence and, in certain conditions, its level might have been moderately but significantly increased even in the absence of prominent, permanent cell cycle arrest at the level of the cell population.

Acknowledgments We would like to acknowledge P. Kopiński, Ph.D. (Department of Gene Therapy, Ludwik Rydygier Collegium Medicum of Bydgoszcz, Nicolaus Copernicus University, Poland) for supplying A549 cells. This work was supported by the Grant UMK (Nicolaus Coprenicus University) no. 33/2008.

Conflict of interest statement None.

References

Akisaka T, Yoshida H, Inoue S, Shimizu K (2001) Organization of cytoskeletal F-actin, G-actin, and gelsolin in the adhesion structures in cultured osteoclast. J Bone Miner Res 16:1248–1255. doi:10.1359/jbmr.2001.16.7.1248

Amaravadi RK, Thompson CB (2007) The roles of therapy-induced autophagy and necrosis in cancer treatment. Clin Cancer Res 13:7271–7279. doi:10.1158/1078-0432.CCR-07-1595

Arthur CR, Gupton JT, Kellogg GE, Yeudall WA, Cabot MC, Newsham IF, Gewirtz DA (2007) Autophagic cell death, polyploidy and senescence induced in breast tumor cells by the substituted pyrrole JG-03–14, a novel microtubule poison. Biochem Pharmacol 74:981–991. doi:10.1016/j.bcp.2007.07.003

Ashcroft M, Vousden KH (1999) Regulation of p53 stability. Oncogene 18:7637–7643. doi:10.1038/sj.onc.1203012

Beauséjour CM, Krtolica A, Galimi F, Narita M, Lowe SW, Yaswen P, Campisi J (2003) Reversal of human senescence: roles of the p53 and p16 pathways. EMBO J 22:4212–4222. doi:10.1093/emboj/cdg417

Binaschi M, Capranico G, Dal Bo L, Zunino F (1997) Relationship between lethal effects and topoisomerase II mediated double-strand DNA breaks produced by anthracyclines with different sequence specificity. Mol Pharmacol 51:1053–1059

Bird J, Ostler EL, Faragher RGA (2003) Can we say that senescent cells cause ageing? Exp Gerontol 38:1319–1326. doi:10.1016/j.exger.2003.09.011

Braig M, Lee S, Loddenkemper C, Rudolph C, Peters AH, Schlegelberger B, Stein H, Dörken B, Jenuwein T, Schmitt CA (2005) Oncogene-induced senescence as an initial barrier in lymphoma development. Nature 436:660–665. doi:10.1038/nature03841

Brookes S, Rowe J, Gutierrez Del Arroyo A, Bond J, Peters G (2004) Contribution of $p16^{INK4a}$ to replicative senescence of human fibroblasts. Exp Cell Res 298:549–559. doi:10.1016/j.yexcr.2004.04.035

Bursch W, Hochegger K, Török L, Marian B, Ellinger A, Hermann RS (2000) Autophagic and apoptotic types of programmed cell death exhibit different fates of cytoskeletal filaments. J Cell Sci 113:1189–1198

Byun Y, Chen F, Chang R, Trivedi M, Green KJ, Cryns VL (2001) Caspase cleavage of vimentin disrupts intermediate filaments and promotes apoptosis. Cell Death Differ 8:443–450. doi:10.1038/sj.cdd.4400840

Cao LG, Fishkind DJ, Wang YL (1993) Localization and dynamics of nonfilamentous actin in cultured cells. J Cell Biol 123:173–181. doi:10.1083/jcb.123.1.173

Chang B-D, Swift ME, Shen M, Fang J, Broude EV, Roninson IB (2002) Molecular determinants of terminal growth arrest induced in tumor cells by a chemotherapeutic agent. Proc Natl Acad Sci USA 99:389–394. doi:10.1073/pnas.012602599

Chen Z, Trotman LC, Shaffer D, Lin H-K, Dotan ZA, Niki M, Koutcher JA, Scher HI, Ludwig T, Gerald W, Cordon-Cardo C, Pandolfi PP (2005) Crucial role of p53-dependent cellular senescence in suppression of Pten-deficient tumorigenesis. Nature 436:725–730. doi:10.1038/nature03918

Colombo R, Necco A, Vailati G, Milzani A (1988) Dose-dependence of doxorubicin effect on actin assembly in vitro. Exp Mol Pathol 49:297–304. doi:10.1016/0014-4800(88)90002-0

Crescenzi E, Palumbo G, Brady HJM (2003) Bcl-2 activates a programme of premature senescence in human carcinoma cells. Biochem J 375:263–274. doi:10.1042/BJ20030868

Crescenzi E, Palumbo G, Brady HJM (2005) Roscovitine modulates DNA repair and senescence: implications for combination chemotherapy. Clin Cancer Res 11:8158–8171. doi:10.1158/1078-0432.CCR-05-1042

Croce MV, Colussi AG, Price MR, Segal-Eiras A (1999) Identification and characterization of different subpopulations in a human lung adenocarcinoma cell line (A549). Pathol Oncol Res 5:197–204. doi:10.1053/paor.1999.0212

Di Felice V, Ardizzone N, Marcianò V, Bartolotta T, Cappello F, Farina F, Zummo G (2005) Senescence-associated HSP60 expression in normal human skin fibroblasts. Anat Rec Discov Mol Cell Evol Biol A 284:446–453

Dimri GP, Lee X, Basile G, Acosta M, Scott G, Roskelley C, Medrano EE, Linskens M, Rubelj I, Pereira-Smith O (1995) A biomarker that identifies senescent human cells in culture and in aging skin in vivo. Proc Natl Acad Sci USA 92:9363–9367. doi:10.1073/pnas.92.20.9363

Dimri GP, Itahana K, Acosta M, Campisi J (2000) Regulation of a senescence checkpoint response by the E2F1 transcription factor and $p14^{ARF}$ tumor suppressor. Mol Cell Biol 20:273–285

Dinsdale D, Lee JC, Dewson G, Cohen GM, Peter ME (2004) Intermediate filaments control the intracellular distribution of caspases during apoptosis. Am J Pathol 164:395–407

Douarre C, Gomez D, Morjani H, Zahm JM, O'donohue MF, Eddabra L, Mailliet P, Riou JF, Trentesaux C (2005) Overexpression of Bcl-2 is associated with apoptotic resistance to the G-quadruplex ligand 12459 but is not sufficient to confer resistance to long-term senescence. Nucleic Acids Res 33:2192–2203. doi:10.1093/nar/gki514

Dulić V, Beney G-E, Frebourg G, Drullinger LF, Stein GH (2000) Uncoupling between phenotypic senescence and cell cycle arrest in aging p21-deficient fibroblasts. Mol Cell Biol 20:6741–6754

Dunaief JL, Strober BE, Guha S, Khavari PA, Alin K, Luban J, Begemann M, Crabtree GR, Goff SP (1994) The retinoblastoma protein and BRG1 form a complex and cooperate to induce cell cycle arrest. Cell 79:119–130. doi:10.1016/0092-8674(94)90405-7

Edelman MJ, Quam H, Mullins B (2001) Interactions of gemcitabine, carboplatin and paclitaxel in molecularly defined non-small-cell lung cancer cell lines. Cancer Chemother Pharmacol 48:141–144. doi:10.1007/s002800000273

Eom Y-W, Kim MA, Park SS, Goo MJ, Kwon HJ, Sohn S, Kim W-H, Yoon G, Choi KS (2005) Two distinct modes of cell death induced by doxorubicin: apoptosis and cell death through mitotic catastrophe accompanied by senescence-like phenotype. Oncogene 24:4765–4777. doi:10.1038/sj.onc.1208627

Eulitz D, Mannherz HG (2007) Inhibition of deoxyribonuclease I by actin is to protect cells from premature cell death. Apoptosis 12:1511–1521. doi:10.1007/s10495-007-0078-4

Fang L, Igarashi M, Leung J, Sugrue MM, Lee SW, Aaronson SA (1999) $p21^{Waf1/Cip1/Sdi1}$ induces permanent growth arrest with markers of replicative senescence in human tumor cells lacking functional p53. Oncogene 18:2789–2797. doi:10.1038/sj.onc.1202615

Feldser DM, Greider CW (2007) Short telomeres limit tumor progression in vivo by inducing senescence. Cancer Cell 11:461–469. doi:10.1016/j.ccr.2007.02.026

Filyak Y, Filyak O, Stoika R (2007) Transforming growth factor beta-1 enhances cytotoxic effect of doxorubicin in human lung adenocarcinoma cells of A549 line. Cell Biol Int 31:851–855. doi:10.1016/j.cellbi.2007.02.008

Filyak Y, Filyak O, Souchelnytskyi S, Stoika R (2008) Doxorubicin inhibits TGF-β signaling in human lung carcinoma A549 cells. Eur J Pharmacol 590:67–73. doi:10.1016/j.ejphar.2008.05.030

Foster KA, Oster CG, Mayer MM, Avery ML, Audus KL (1998) Characterization of the A549 cell line as a type II pulmonary epithelial cell model for drug metabolism. Exp Cell Res 243:359–366. doi:10.1006/excr.1998.4172

Giard DJ, Aaronson SA, Todaro GJ, Arnstein P, Kersey JH, Dosik H, Parks WP (1973) In vitro cultivation of human tumors:

establishment of cell lines derived from a series of solid tumors. J Natl Cancer Inst 51:1417–1423

Grzanka A, Grzanka D, Orlikowska M (2003) Cytoskeletal reorganization during process of apoptosis induced by cytostatic drugs in K-562 and HL-60 leukemia cell lines. Biochem Pharmacol 66:1611–1617. doi:10.1016/S0006-2952(03)00532-X

Guénal I, Risler Y, Mignotte B (1997) Down-regulation of actin genes precedes microfilament network disruption and actin cleavage during p53-mediated apoptosis. J Cell Sci 110:489–495

Hatcher EL, Alexander JM, Kang YJ (1997) Decreased sensitivity to adriamycin in cadmium-resistant human lung carcinoma A549 cells. Biochem Pharmacol 53:747–754. doi:10.1016/S0006-2952(96)00811-8

Haynes A, Shaik MS, Chatterjee A, Singh M (2003) Evaluation of an aerosolized selective COX-2 inhibitor as a potentiator of doxorubicin in a non-small-cell lung cancer cell line. Pharm Res 20:1485–1495. doi:10.1023/A:1025774630993

He Y, Fan S, Jiang Y (2005) p73 gene overexpression induces apoptosis and increases chemosensitivity in human lung adenocarcinoma cells A549. Int J Oncol 3:1

Hoffman PC, Mauer AM, Vokes EE (2000) Lung cancer. Lancet 355:479–485

Hukkanen J, Lassila A, Päivärinta K, Valanne S, Sarpo S, Hakkola J, Pelkonen O, Raunio H (2000) Induction and regulation of xenobiotic-metabolizing cytochrome P450 s in the human A549 lung adenocarcinoma cell line. Am J Respir Cell Mol Biol 22:360–366

Iavarone A, Massagué J (1997) Repression of the CDK activator Cdc25A and cell-cycle arrest by cytokine TGF-β in cells lacking the CDK inhibitor p15. Nature 387:417–422. doi:10.1038/387417a0

Kamijo T, Zindy F, Roussel MF, Quelle DE, Downing JR, Ashmun RA, Grosveld G, Sherr CJ (1997) Tumor suppression at the mouse *INK4a* locus mediated by the alternative reading frame product $p19^{ARF}$. Cell 91:649–659. doi:10.1016/S0092-8674(00)80452-3

Katakura Y, Nakata E, Miura T, Shirahata S (1999) Transforming growth factor β triggers two independent-senescence programs in cancer cells. Biochem Biophys Res Commun 255:110–115. doi:10.1006/bbrc.1999.0129

Klein LE, Freeze BS, Smith AB, Horwitz SB (2005) The microtubule stabilizing agent discodermolide is a potent inducer of accelerated senescence. Cell Cycle 4:501–507

Kurz DJ, Decary S, Hong Y, Erusalimsky JD (2000) Senescence-associated β-galactosidase reflects an increase in lysosomal mass during replicative ageing of human endothelial cells. J Cell Sci 113:3613–3622

Kwak IH, Kim HS, Choi OR, Ryu MS, Lim IK (2004) Nuclear accumulation of globular actin as a cellular senescence marker. Cancer Res 64:572–580. doi:10.1158/0008-5472.CAN-03-1856

Lee BY, Han JA, Im JS, Morrone A, Johung K, Goodwin EC, Kleijer WJ, DiMaio D, Hwang ES (2006) Senescence-associated β-galactosidase is lysosomal β-galactosidase. Aging Cell 5:187–195. doi:10.1111/j.1474-9726.2006.00199.x

Lieber M, Smith B, Szakal A, Nelson-Rees W, Todaro G (1976) A continuous tumor-cell line from a human lung carcinoma with properties of type II alveolar epithelial cells. Int J Cancer 17:62–70. doi:10.1002/ijc.2910170110

Lim IK, Hong KW, Kwak IH, Yoon G, Park SC (2000) Cytoplasmic retention of p-Erk1/2 and nuclear accumulation of actin proteins during cellular senescence in human diploid fibroblasts. Mech Ageing Dev 119:113–129. doi:10.1016/S0047-6374(00)00167-6

Liu Y, El-Naggar S, Darling DS, Higashi Y, Dean DC (2008) Zeb1 links epithelial-mesenchymal transition and cellular senescence. Development 135:579–588. doi:10.1242/dev.007047

Lock RB, Stribinskiene L (1996) Dual modes of death induced by etoposide in human epithelial tumor cells allow Bcl-2 to inhibit apoptosis without affecting clonogenic survival. Cancer Res 56:4006–4012

Lockshin RA, Zakeri Z (2004) Apoptosis, autophagy, and more. Int J Biochem Cell Biol 36:2405–2419. doi:10.1016/j.biocel.2004.04.011

Mashima T, Naito M, Noguchi K, Miller DK, Nicholson DW, Tsuruo T (1997) Actin cleavage by CPP-32/apopain during the development of apoptosis. Oncogene 14:1007–1012. doi:10.1038/sj.onc.1200919

Meijerman I, Blom WM, de Bont HJGM, Mulder GJ, Nagelkerke JF (1997) Nuclear accumulation of G-actin in isolated rat hepatocytes by adenine nucleotides. Biochem Biophys Res Commun 240:697–700. doi:10.1006/bbrc.1997.7724

Meijerman I, Blom WM, de Bont HJGM, Mulder GJ, Nagelkerke JF (1999) Induction of apoptosis and changes in nuclear G-actin are mediated by different pathways: the effect of inhibitors of protein and RNA synthesis in isolated rat hepatocytes. Toxicol Appl Pharmacol 156:46–55. doi:10.1006/taap.1998.8616

Meriwether WD, Bachur NR (1972) Inhibition of DNA and RNA metabolism by daunorubicin and adriamycin in L1210 mouse leukemia. Cancer Res 32:1137–1142

Mi J, Zhang X, Rabbani ZN, Liu Y, Reddy SK, Su Z, Salahuddin FK, Viles K, Giangrande PH, Dewhirst MW, Sullenger BA, Kontos CD, Clary BM (2008) RNA aptamer-targeted inhibition of NF-κB suppresses non-small cell lung cancer resistance to doxorubicin. Mol Ther 16:66–73. doi:10.1038/sj.mt.6300320

Michaloglou C, Vredeveld LCW, Soengas MS, Denoyelle C, Kuilman T, van der Horst CM, Majoor DM, Shay JW, Mooi WJ, Peeper DS (2005) $BRAF^{E600}$-associated senescence-like cell cycle arrest of human naevi. Nature 436:720–724. doi:10.1038/nature03890

Michishita E, Nakabayashi K, Ogino H, Suzuki T, Fujii M, Ayusawa D (1998) DNA topoisomerase inhibitors induce reversible senescence in normal human fibroblasts. Biochem Biophys Res Commun 253:667–671. doi:10.1006/bbrc.1998.9832

Milzani A, Rossi R, Di Simplicio P, Giustarini D, Colombo R, DalleDonne I (2000) The oxidation produced by hydrogen peroxide on Ca-ATP-G-actin. Protein Sci 9:1774–1782. doi:10.1110/ps.9.9.1774

Mishima K, Handa JT, Aotaki-Keen A, Lutty GA, Morse LS, Hjelmeland LM (1999) Senescence-associated β-galactosidase histochemistry for the primate eye. Invest Ophthalmol Vis Sci 40:1590–1593

Moll UM, Ostermeyer AG, Haladay R, Winkfield B, Frazier M, Zambetti G (1996) Cytoplasmic sequestration of wild-type p53 protein impairs the G1 checkpoint after DNA damage. Mol Cell Biol 16:1126–1137

Mortenson MM, Schlieman MG, Virudachalam S, Bold RJ (2004) Effects of the proteasome inhibitor bortezomib alone and in combination with chemotherapy in the A549 non-small-cell lung cancer cell line. Cancer Chemother Pharmacol 54:343–353. doi:10.1007/s00280-004-0811-4

Moxham BL, Webb PP, Benjamin M, Ralphs JR (1998) Changes in the cytoskeleton of cells within the periodontal ligament and dental pulp of the rat first molar tooth during ageing. Eur J Oral Sci 106(Suppl 1):376–383

Nakanishi K, Maruyama M, Shibata T, Morishima N (2001) Identification of a caspase-9 substrate and detection of its cleavage in programmed cell death during mouse development. J Biol Chem 276:41237–41244. doi:10.1074/jbc.M105648200

Narita M, Nũnez S, Heard E, Narita M, Lin AW, Hearn SA, Spector DL, Hannon GJ, Lowe SW (2003) Rb-mediated heterochromatin formation and silencing of E2F target genes during cellular senescence. Cell 113:703–716. doi:10.1016/S0092-8674(03)00401-X

Nishio K, Inoue A (2005) Senescence-associated alterations of cytoskeleton: extraordinary production of vimentin that anchors

cytoplasmic p53 in senescent human fibroblasts. Histochem Cell Biol 123:263–273. doi:10.1007/s00418-005-0766-5

Nishio K, Inoue A, Qiao S, Kondo H, Mimura A (2001) Senescence and cytoskeleton: overproduction of vimentin induces senescent-like morphology in human fibroblasts. Histochem Cell Biol 116:321–327. doi:10.1007/s004180100325

Okamoto A, Hussain SP, Hagiwara K, Spillare EA, Rusin MR, Demetrick DJ, Serrano M, Hannon GJ, Shiseki M, Zariwala M, Xiong Y, Beach DH, Yokota J, Harris CC (1995) Mutations in the $p16^{INK4}$/*MTS1*/*CDKN2*, $p15^{INK4B}$/*MTS2*, and *p18* genes in primary and metastatic lung cancer. Cancer Res 55:1448–1451

Olave IA, Reck-Peterson SL, Crabtree GR (2002) Nuclear actin and actin-related proteins in chromatin remodeling. Annu Rev Biochem 71:755–781. doi:10.1146/annurev.biochem.71.110601.135507

Otterson GA, Villalona-Calero MA, Sharma S, Kris MG, Imondi A, Gerber M, White DA, Ratain MJ, Schiller JH, Sandler A, Kraut M, Mani S, Murren JR (2007) Phase I study of inhaled doxorubicin for patients with metastatic tumors to the lungs. Clin Cancer Res 13:1246–1252. doi:10.1158/1078-0432.CCR-06-1096

Parkin MD (2001) Global cancer statistics in the year 2000. Lancet Oncol 2:533–543. doi:10.1016/S1470-2045(01)00486-7

Patlakas G, Bouros D, Tsantekidou-Pozova S, Koukourakis MI (2005) Triplet chemotherapy with docetaxel, gemcitabine and liposomal doxorubicin, supported with subcutaneous amifostine and hemopoietic growth factors, in advanced non-small cell lung cancer. Anticancer Res 25:1427–1431

Pendleton A, Pope B, Weeds A, Koffer A (2003) Latrunculin B or ATP depletion induces cofilin-dependent translocation of actin into nuclei of mast cells. J Biol Chem 278:14394–14400. doi:10.1074/jbc.M206393200

Pronzato P, Vigani A, Tognoni A, Vaira F, Canessa P (2001) Anthracyclines in non-small cell lung cancer. Lung Cancer 34:S57–S59. doi:10.1016/S0169-5002(01)00394-4

Rando OJ, Zhao K, Janmey P, Crabtree GR (2002) Phosphatidylinositol-dependent actin filament binding by the SWI/SNF-like BAF chromatin remodeling complex. Proc Natl Acad Sci USA 99:2824–2829. doi:10.1073/pnas.032662899

Rebbaa A (2005) Targeting senescence pathways to reverse drug resistance in cancer. Cancer Lett 219:1–13. doi:10.1016/j.canlet.2004.08.011

Rebbaa A, Zheng X, Chou PM, Mirkin BL (2003) Caspase inhibition switches doxorubicin-induced apoptosis to senescence. Oncogene 22:2805–2811. doi:10.1038/sj.onc.1206366

Riou JF, Guittat L, Mailliet P, Laoui A, Renou E, Petitgenet O, Mégnin-Chanet F, Hélène C, Mergny JL (2002) Cell senescence and telomere shortening induced by a new series of specific G-quadruplex DNA ligands. Proc Natl Acad Sci USA 99:2672–2677. doi:10.1073/pnas.052698099

Roberson RS, Kussick SJ, Vallieres E, Chen SY, Wu DY (2005) Escape from therapy-induced accelerated cellular senescence in p53-null lung cancer cells and in human lung cancers. Cancer Res 65:2795–2803. doi:10.1158/0008-5472.CAN-04-1270

Safiejko-Mroczka B, Bell PB (1998) Distribution of cytoskeletal proteins in neomycin-induced protrusions of human fibroblasts. Exp Cell Res 242:495–514. doi:10.1006/excr.1997.3871

Schmitt CA, Fridman JS, Yang M, Lee S, Baranov E, Hoffman RM, Lowe SW (2002) A senescence program controlled by p53 and $p16^{INK4a}$ contributes to the outcome of cancer therapy. Cell 109:335–346. doi:10.1016/S0092-8674(02)00734-1

Seluanov A, Gorbunova V, Falcovitz A, Sigal A, Milyavsky M, Zurer I, Shohat G, Goldfinger N, Rotter V (2001) Change of the death pathway in senescent human fibroblasts in response to DNA damage is caused by an inability to stabilize p53. Mol Cell Biol 21:1552–1564. doi:10.1128/MCB.21.5.1552-1564.2001

Sherwood SW, Rush D, Ellsworth JL, Schimke RT (1988) Defining cellular senescence in IMR-90 cells: a flow cytometric analysis. Proc Natl Acad Sci USA 85:9086–9090. doi:10.1073/pnas.85.23.9086

Sommers CL, Heckford SE, Skerker JM, Worland P, Torri JA, Thompson EW, Byers SW, Gelmann EP (1992) Loss of epithelial markers and acquisition of vimentin expression in adriamycin- and vinblastine-resistant human breast cancer cell lines. Cancer Res 52:5190–5197

Spira A, Ettinger DS (2004) Multidisciplinary management of lung cancer. N Engl J Med 350:379–392. doi:10.1056/NEJMra035536

Stein GH, Drullinger LF, Soulard A, Dulić V (1999) Differential roles for cyclin-dependent kinase inhibitors p21 and p16 in the mechanisms of senescence and differentiation in human fibroblasts. Mol Cell Biol 19:2109–2117

Sung J-M, Cho H-J, Yi H, Lee CH, Kim HS, Kim DK, Abd El-Aty AM, Kim JS, Landowski CP, Hediger MA, Shin HC (2008) Characterization of a stem cell population in lung cancer A549 cells. Biochem Biophys Res Commun 371:163–167. doi:10.1016/j.bbrc.2008.04.038

te Poele RH, Okorokov AL, Jardine L, Cummings J, Joel SP (2002) DNA damage is able to induce senescence in tumor cells in vitro and in vivo. Cancer Res 62:1876–1883

Thomson S, Buck E, Petti F, Griffin G, Brown E, Ramnarine N, Iwata KK, Gibson N, Haley JD (2005) Epithelial to mesenchymal transition is a determinant of sensitivity of non-small-cell lung carcinoma cell lines and xenografts to epidermal growth factor receptor inhibition. Cancer Res 65:9455–9462. doi:10.1158/0008-5472.CAN-05-1058

Tolstonog GV, Shoeman RL, Traub U, Traub P (2001) Role of the intermediate filament protein vimentin in delaying senescence and in the spontaneous immortalization of mouse embryo fibroblasts. DNA Cell Biol 20:509–529. doi:10.1089/104454901317094945

Untergasser G, Koch HB, Menssen A, Hermeking H (2002) Characterization of epithelial senescence by serial analysis of gene expression: identification of genes potentially involved in prostate cancer. Cancer Res 62:6255–6262

Van der Loo B, Fenton MJ, Erusalimsky JD (1998) Cytochemical detection of a senescence-associated β-galactosidase in endothelial and smooth muscle cells from human and rabbit blood vessels. Exp Cell Res 241:309–315. doi:10.1006/excr.1998.4035

Vartiainen MK, Guettler S, Larijani B, Treisman R (2007) Nuclear actin regulates dynamic, subcellular localization and activity of the SRF cofactor MAL. Science 316:1749–1752

Wada A, Fukuda M, Mishima M, Nishida E (1998) Nuclear export of actin: a novel mechanism regulating the subcellular localization of a major cytoskeletal protein. EMBO J 17:1635–1641. doi:10.1093/emboj/17.6.1635

Walen KH (2007) Origin of diplochromosomal polyploidy in near-senescent fibroblast cultures: Heterochromatin, telomeres and chromosomal instability (CIN). Cell Biol Int 31:1447–1455. doi:10.1016/j.cellbi.2007.06.015

Wang X, Wong SCH, Pan J, Tsao SW, Fung KHY, Kwong DLW, Sham JST, Nicholls JM (1998) Evidence of cisplatin-induced senescent-like growth arrest in nasopharyngeal carcinoma cells. Cancer Res 58:5019–5022

Węsierska-Gądek J, Wojciechowski J, Ranftler C, Schmid G (2005) Role of p53 tumor suppressor in ageing: regulation of transient cell cycle arrest and terminal senescence. J Physiol Pharmacol 56:15–28

Xie QC, Hu YD, Wang LL, Chen ZT, Diao XW, Wang ZX, Guan HJ, Zhu B, Sun JG, Duan YZ, Chen FL, Nian WQ (2005) The co-transfection of p16(INK4a) and p14(ARF) genes into human lung cancer cell line A549 and the effects on cell growth and

chemosensitivity. Colloids Surf B Biointerfaces 46:188–196. doi:10.1016/j.colsurfb.2005.10.006

Yang D, McCrann DJ, Nguyen H, St Hilaire C, DePinho RA, Jones MR, Ravid K (2007) Increased polyploidy in aortic vascular smooth muscle cells during aging is marked by cellular senescence. Aging Cell 6:257–260. doi:10.1111/j.1474-9726.2007.00274.x

Zhang R, Chen W, Adams PD (2007) Molecular dissection of formation of senescence-associated heterochromatin foci. Mol Cell Biol 27:2343–2358. doi:10.1128/MCB.02019-06